Project Final Report

Grant Agreement number: 295823

Project acronym: PROCARDIO

Project title: Cardiovascular Risk from Exposure to Low-dose and Low-dose-rate Ionizing Radiation

Funding Scheme: Collaborative Project

Date of latest version of Annex I against which the assessment will be made: 03.09.2014

Period covered: from October 1, 2011 to March 31, 2015

Name, title and organisation of the scientific representative of the project's coordinator:

Prof. Michael John Atkinson
Helmholtz Center Munich GmbH

Tel: +49 89 31872983
Fax: +49 89 31873378
E-mail: atkinson@helmholtz-muenchen.de

Project website address: www.procardio.eu

Table of Content

Final publishable summary report

PROCARDIO

Logo:

Project title: Cardiovascular Risk from Exposure to Low-dose and Low-dose-rate Ionizing Radiation

Website: www.procardio.eu

Contractors involved (PROCARDIO consortium):

Name and address of coordinator:

Prof. Michael John Atkinson

Helmholtz Center Munich GmbH

Institute of Radiation Biology

Ingolstaedter Landstr. 1

85764 Neuherberg, Germany

Other partners and team leaders:

Partner 02: CREAL, Fundacio Centre de Recerca en Epidemiologia Ambiental, Spain

Partner 03: IGR, Institut Gustave Roussy, France

Partner 04: GSI, Helmholtzzentrum fuer Schwerionenforschung GmbH

Partner 05: HPA, Health Protection Agency

Partner 06: ENEA, Agenzia Nazionale per le Nuove Tecnologie, L'Energia e lo Sviluppo Economico Sostenibile, Italy

Partner 07: SCK-CEN, Studiencentrum voor Kernenergie, Belgium

Partner 08: GABO:mi, Gesellschaft fuer Ablauforgansiation :milliarium mbH & Co. KG, Germany

Partner 09: UB, The University of Birmingham, UK

Partner 10: RIVM, Rijksinstituut voor Volksgezondheiden Milieu, Netherlands

Partner 11: SUBI, Southern Urals Biophysics Institute of Federal Medicobiological Agency, Russia

Partner 12: AMC, Academisch Medisch Centrum bij de Universiteit van Amsterdam, Netherlands

Partner 13: DH-PHE, Department of Health, Public Health England, UK

1.1 Executive summary

Since the earliest years of radiation research the heart was always considered to be a radioresistant organ, with textbooks indicating a tolerance dose of 20 Gy. Towards the end of the 20th century epidemiological studies of cancer and A-bomb survivors, as well as nuclear workers, provided the first indications that long-term damage to the heart and vessels could occur at radiation doses considerably below 2 Gy. This prompted a number of new investigations that have convincingly demonstrated risks of adverse health effects to the heart in those receiving doses in the moderate (above 500mGy) range. Two competing opinions exist on the risks at doses below 500mGy. The deterministic viewpoint considers that there may be a dose (threshold) below which there is no damage and no risk of cardiovascular disease. The alternative standpoint suggests that the dose declines continually without a threshold. Thus a risk will exist even at doses far below 500mGy. The unresolvable uncertainties inherent to these epidemiological studies allow both interpretations, although there has recently been a non-significant trend reported in favour of the linear non-threshold relationship and risks detectable in the 100-250 mGy range. The gaps in our knowledge of radiation and the heart remains one of the most pressing question in radiation protection. This is especially true as exposure to the heart is an almost unavoidable part of modern life, with low doses coming from medical imaging (CT, PET, and X-rays), from tumour therapy, and from both the workplace and natural sources.

The key findings of ProCardio

I) An epidemiological case-control study of the risk of cardiac disease following low dose exposures has been recruited, made up of 222 survivors of childhood cancer who later developed cardiac diseases and an equal number of survivors who did not developed cardiac disease. The initial analysis provides evidence for a dose-dependent risk of cardiovascular disease following radiation exposure.

II) The case-control study will be pooled with a case-control study conducted within a larger pan-European study of the health of Childhood Cancer Survivors (PanCareSurF). The pooled ProCardio / PanCareSurF study will include 900 cases and 900 controls.

III) There is evidence for a cardiovascular relative biological effectiveness (RBE_{CVD}), with an estimated value of between 4 and 10 for HZE irradiation compared to photons.

IV) Differences in the response of surrogate markers of cardiovascular disease to low dose rate and acute exposures provide evidence that a dose and dose rate correction factor ($DDREF_{CVD}$) should be considered for cardiovascular tissue.

V) There is evidence for the existence of a modest abscopal effect, where partial body exposure may increase atherosclerotic plaque formation in non-irradiated vessels of the heart.

VI) Cellular interactions are important for the development of radiation-induced atherosclerosis. Radiation accelerates the process by stimulating both monocyte adhesion to, and the infiltration of lipids through, the endothelium.

VII) MicroRNAs as well as both de-acetylated and mitochondrial respiration complex proteins are indicated as potential biomarkers of radiation-induced heart disease.

VIII) Two mathematical models of radiation action have been generated. These show a good fit with experimental data. One model predicts that plaque initiation and not plaque expansion is the key process in radiation-induced heart disease. The other model, when fitted to A-Bomb survivor data indicates a non-linearity of the dose response relationship towards higher doses.

1.2 Summary description of project context and objectives:

Background and Aims

The damaging effects of high doses of radiation on the heart have been recognized from histo-pathological analysis, showing damage to the valvular system, the pericardium and the muscle. Nevertheless, the heart has historically been considered as a radio-resistant organ, with a tolerance dose estimated in the 20 Gy range. Recent epidemiological evidence has challenged this, and demonstrate that an increased risk of cardiovascular disease is associated with exposures in the moderate dose range, considerably below 2 Gy. The long-term consequences of exposure to even lower doses of radiation, typically those received by radiation workers, from repeated medial imaging procedures or from contact with the natural environment, remain uncertain. It is precisely these doses and exposure situations where society has the greatest need for definitive information on the risk to the cardiovascular system. The same problems also arise in considering effects of radiation on the brain, and hence ProCardio is strategically and scientifically aligned with the EU project CEREBRAD, sharing information, technology and concepts to create a synergy between the projects.

Work strategy and general description

ProCardio is designed to advance knowledge of the cardiovascular risks at low doses through a dual approach involving both epidemiology and the understanding/modelling of the dose response relationship. Work Package 3 concerns a case-control study of cardiac diseases nested within cohorts of cancer survivors from France, the UK and Spain. The key aspects of this study has been the collection of clinical and questionnaire data detailing potential confounders and a much improved individual dosimetry.

Work packages 4-8 address major biological questions on the cardiovascular effects of low dose and dose rate radiation. In workpackage 4 the possible effects of different radiation qualities, in workpackage 5 the effect of different dose rates, in work-package 6 the importance of cell-cell communication were studied. In workpackage 7 we conducted high throughput Omics analysis for other workpackages and also addressed the issue of radiation biomarkers and in workpackage 8 we have developed new modelling strategies to describe the dose response relationship.

Management structure and procedures

The Project Coordinator ensured the smooth operation of the project and guaranteed that all efforts were focused towards the objectives. He submitted all required progress reports, deliverables, financial statements to the European Commission, and, with the assistance of GABO:mi he was responsible for the proper use of funds and their transfers to participants. The PROCARDIO office was established by and based at the coordinator in Munich, Germany and at GABO:mi in Munich. The Project Office at the Coordinator was concerned with the scientific management and the co-ordination of all research activities. The Project Office at GABO:mi was responsible for administrative, financial and contractual management and the organisational co-ordination of the project activities.

The Project Governing Board, i.e. the General Assembly, was in charge of the political and strategic orientation of the project and acted as the arbitration body. It met once a year. The Project Management Board consisted of all work package leaders and the Coordinator and was in charge of monitoring all activities towards the objective of the project in order to deliver as promised, in due time and in the budget. The Management Board met every six months during the funding period. Furthermore, a scientific advisory board was implemented to ensure a high standard of research and monitor the progress of the project by taking part in the annual Governing Board Meetings.

Objectives of PROCARDIO:
In order to improve understanding of the risks of cardiovascular disease at low doses we undertook to:
- Design an epidemiological study of survivors of childhood cancer.
- Investigate the action of low doses and low dose rates on the heart and vessels.
- Conduct a search for biological markers of low dose effects on heart.
- Evolve mathematical procedures to better describe the dose response relationship.

1.3 Description of the main S&T results/foregrounds of PROCARDIO

1.3.1 Case-control study of the risks of low dose radiation for the cardiovascular system

1.3.1.1 Study design

We have conducted a new epidemiological case-control study by retrospectively evaluating cardiovascular events in 3 cohorts of childhood cancer survivors. By early 2015 we assembled a European case-control study of 225 long-term survivors of childhood cancer with at least one cardiovascular event (stable angina, unstable angina, heart failure etc.) (130 cases from the French Childhood Cancer Survivors Study (FCCSS), 82 from the British Childhood Cancer Survivors Study (BCCSS) and a further 13 from the newly created Catalonian Cancer Survivors Study[1]. Appropriate matched controls were identified based upon, country, gender, age at first diagnosis, year of diagnosis, and length of follow-up. To date, a total of 13 cases were identified and accepted to participate. Of these, only 10 are included in the statistical analysis as detailed information about the cardiac event was not yet available at the time the analysis was conducted. The ProCardio case-control study is conducted in parallel to a EU-Health FP7 study that aims to recruit an additional 600 cases and 600 controls, PanCareSurF (PCSF; coordinator Lars Hjorth, University of Lund, Sweden).

1.3.1.2 Data providers

IGR identified all cases of cardiac diagnosed in patients from the French Childhood Cancer Survivors (FCCSS), which had not yet been previously included in the PCSF Project, and which occurred in childhood cancer patients who survived at least 5 years from diagnosis. Cardiac diseases were identified and by self-questionnaire, access to medical records and linkage with the French National Hospital and Health Insurance Data Base (SNIIR-AM). **UB** undertook to identify all cases of serious cardiac disease diagnosed before 1993 among individuals diagnosed with childhood cancer between 1940 and 1991, in Britain, and surviving at least 5 years from diagnosis. Full details of chemotherapy and radiotherapy from the original treatment hospitals have been obtained for 84 matched sets, corresponding to 82 patients having developed at least one cardiac disease. For reasons beyond the control of the Beneficiary **CREAL** the originally planned Spanish Childhood Cancer Survivor Study could not be set-up during the study period. An alternative study, for the autonomous region of Cataluña, has been initiated. This has resulted in the identification of 13 cases (10 included in the ProCardio analysis) to date. The planned final number will be delivered for the PancareSurF analysis. The **AMC** has been responsible for the strategic collaboration with PanCareSurF (PCSF) and for ensuring standardization across the two projects. The method of ascertainment and validation of cardiac events in ProCardio was developed in collaboration with PCSF WP3. AMC also supported the other ProCardio partners by providing clinical cardiology expertise.

1.3.1.3 The ProCardio Case-Control study

A total 222 patients with at least one cardiac pathologies (a total of 240) have been identified by the 3 data providers. Table 1 describes the cases of cardiac disease included in the WP3 case-control study. Heart failure is an evolution of most of the cardiac diseases and may be an evolution of ischemic diseases, pericarditis, and valvular disease of arrhythmia. Therefore, to be coded in heart failure or any of these disease depends of the stage of cardiac diseases at the diagnosis. One control from the same national cohort was matched to each case by gender; age at first primary cancer diagnosis (+/- 1 year); calendar year at first primary cancer diagnosis (+/- 3 years) and length of follow-up.

1.3.1.4 Whole body dosimetric reconstruction

For dose reconstructions in the ProCardio project, the IGR team has adapted its retrospective dose reconstruction system in order to achieve the specifications of the study. The main components of the IGR dosimetry system are a library of voxel-based anthropomorphic phantoms enabling simulations of the patient whole body and a dose calculation software capable of evaluating both the high doses delivered to the radiotherapy target volume and the low doses to remote organs because of unavoidable secondary radiations mainly originating from scattering in the patient or the beam limiting device and also machine leakage

[1] Additional cases will be added in the next months to complete the original complement of 300 cases and 300 controls

Table 1– Characteristics of the patients having at least one cardiac pathology in the ProCardio case-control study.

	France	UK	Spain	Whole study
Patients: cases	130	82	10	222
Type of cardiac diseases				
Heart failure	63	24	4	92
Ischemic diseases	9	43	1	53
Pericarditis	14	0	1	15
Valvular diseases	29	10	1	40
Arrhythmia	9	7	2	18
Other or Non Specified	22	0	0	22
Gender				
Female	61	47	3	113
Male	69	35	7	109
Birth year, mean (min-max)	1979 (1961-1997)	1961 (1936-1989)	1983 (1976-1991)	1973 (1936-1997)
Cancer Diagnostic date, mean (min-max)	1988 (1974-2000)	1969 (1940-1991)	1988 (1975-1995)	1981 (1940-2000)
Age at cancer diagnosis, mean (min-max)	8 (0-19)	8 (0-15)	7 (0-16)	9 (0-19)
Cardiac disease diagnostic date, mean (min-max)	2000 (1981-2014)	1996 (1967-2002)	2004 (1989-2013)	1998 (1967-2014)
Delay between cancer and CVD diagnosis	12 (0-35)	26 (5-59)	9 (0-27)	17 (0-59)
Age at cardiac disease diagnosis, mean (min-max)	20 (0.4-52.3)	34 (11-61)	16(10-30)	26 (0.4-61)

Concerning the phantoms, the most important adaptation for the ProCardio project was a finer segmentation of the heart volume and sub-volumes. As a result, the phantoms now include a 3D representation of 14 sub-structures in the heart. These are: the cardiac muscle, the left and right ventricles, the left and right atriums, the left anterior descending arteries, the left circumflex artery, the right coronary artery, the aortic valve, the pulmonary valve, the mitral valve and the tricuspid valve, the interventricular septum and the pericardium. To date, we have achieved the dose reconstructions for 138 of the 141 cases that had received radiation therapy and for 113 of the 120 controls that had received radiotherapy. Not all cases and controls from Spain were included in this analysis due to timing of the collection of data. For each of these patients, the IGR collected clinical parameters, including sex, age, height, weight, and any available data on external measurements that could be obtained from treatment planning charts. We abstracted each patient's RT parameters, including target-volume locations, prescribed dose, number of fields, field configuration(s), field size(s), type of treatment machine, beam energies, and other parameters. This enabled highly individualised dose reconstructions as close as possible to actual treatment conditions of each subject (Figure 1).

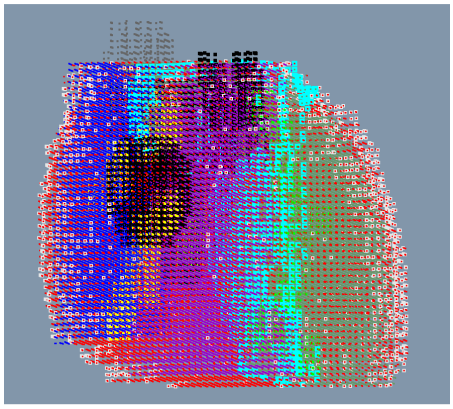

Figure 1 – A 3D representation of the voxels available at heart level for the calculation of the heart sub- structures doses distributions in the case of a 17 years aged male patient.

1.3.1.5 Evaluation of risk of ischemic heart diseases for all types of cardiac pathologies

In a multivariate conditional logistic regression analysis including treatment factors, anthracycline administration increased (p=0.0004) by a factor of 3.78 (95%CI: 1.88to 7.58) the risk of cardiac disease, whereas alkylating agent administration was associated to a near from significant (p=0.1) increase of risk: 0R=1.87 (95%CI: 0.95 to 3.66). A significant (p<0.0001) increase in risk of cardiac disease was observed when increasing the average radiation dose received to the heart.

When considering the role of the average radiation dose in the risk of cardiac diseases, all together, the best model fitting the data was an exponential model (Table 2). The estimated Excess of Odds Ratio at 1Gy (EOR/Gy) of average heart radiation dose was 0.083 (95%CI: 0.051-0.12). The risk estimate was similar in analyses restricted to ischemic diseases (EOR/Gy=0.068, 95%CI: 0.0 to 0.14), heart failure (which are, for most of them of ischemic origin) or all ischemic diseases together (EOR/Gy= 0.076 (95%CI: 0.034 to 0.12)) (Table 2).

In analyses restricted to subjects with doses below 1 Gy, results suggest a higher risk: EOR/Gy = 1.31 (95%CI: -0.90 to 13.3) for all cardiac diseases as a group and EOR/1Gy = 1.50 (95%CI: 0.21 to 33.27) for the risk of ischemic heart diseases or heart failure as a function of average dose to the left anterior descending artery. These results, however, are based on small numbers and the confidence intervals are very large. These findings should be verified, as planed in the ProCardio protocol, by pooling the ProCardio and PCSF case-control studies, thus increasing the statistical power since by including a total of 900 cardiac diseases following childhood cancer and 900 controls.

Table 2 – Risk factors for all cardiac diseases (multivariate conditional regression).

	EOR/Gy (95%CI)	β (95%CI)	Deviance
Model			
Constant			264.71
Linear : OR=Cst (1°+ α dose)	0.13 (0.048 ; 0.32)		243.52
Quadratic: OR=Cst (1°+ α dose*dose)	0.0046 (0.0016-0.011)		242.73
Exponential: OR=Cst (1°+ exp α dose)	0.083 (0.051-0.12)		240.38
LQ : OR=Cst (1°+ α dose + β dose*dose)	0.04 (-0.10 ; 0.30)	0.0034 (-0.052; 0.01)	243.50

1.3.1.6 Summary of ProCardio epidemiological results

The analysis of 222 patients having experienced cardiac diseases provides some results that improve the knowledge about the risk of radiation induced cardiac disease.

When considering the role of the average radiation dose in the risk of cardiac diseases, all together, the best model was an exponential model and the estimated EOR/Gy was 0.083 (95%CI: 0.051-0.12), no interaction was observed with anthracycline administration. The risk estimate was similar for ischemic diseases and heart failure. There was a suggestion of a higher risk in analyses restricted to subjects with less than 1 Gy on average to the heart.

It should be noted that, when considering the average heart radiation dose, though not based on the same dose-response model, our results are very similar those obtained in a study of adult women treated for a breast cancer, EOR/Gy =0.074 (95%CI: 0.029 to 0.145) (Darby et al. 2013), as well as in a meta-analysis of studies investing cardiac diseases risk following low dose exposure, ERR/1Gy=0.10 (95%CI: 0.04to 0.15) (Little et al. 2012).

All these findings need to be verified, as planed in the ProCardio protocol, by pooling the ProCardio case-control study, with the PCSF one in order to reach a sufficient power by including a total of 900 cardiac diseases following childhood cancer and 900 controls.

1.3.2 Effects of radiation quality

We have investigated the efficiency of high LET radiation and to determine if the current values for the Relative Biological Effectiveness (RBE) are applicable to radiation vascular damage. High LET Fe ions and X-ray irradiation as a reference was used for the investigation of the radiation induced changes.

1.3.2.1 Strategy to identify possible RBE effects on cardiovascular tissues

Two cell models, representing endothelial cells and vascular smooth muscle cells, were selected to compare high and low LET effects on relevant cardiovascular phenotypes. We have used hTERT immortalized human coronary arteries (EC). For a major part of the investigations, hTERT established human smooth muscle cells (SMC) and, for some experiments, a co-culture of EC grown on a monolayer of SMC, were used. Photon irradiations (X-ray, 250 kV, 13 mA) were carried out in the respective laboratories of the partners separately. Charged particle exposures (Fe ions, 1GeV/u, 155 keV/µm) were performed in a single pilot experiment by the GSI for all investigations. Cells were exposed in a confluent state to radiation doses between 0.05 and 2 Gy (either X-rays or Fe ions). For Fe ion exposure, the percentage of cell nuclei traversed was calculated based on the nuclear surface (EC 170 μm^2 ± 22; SMC 270 μm^2 ± 83) and the fluence (0.05 Gy = 2.1 x 10^3 P/cm^2). The fraction of cells traversed by at least one particle is 40% for EC and 60% for SMC.

1.3.2.2 Results of the evaluation of a possible RBE for high LET in cardiovascular models

1.3.2.2.1 Transcriptomics analysis after high and low LET irradiation

Microarray analysis (Affymetrix Human Gene 2.0 ST Array Chips) was performed by SCK-CEN with total RNA of irradiated ECs. Raw affymetrix data were imported into the Partek Genomics Suite v6.6 software (Partek Inc.). To test for differential expression two-way ANOVA analysis (with time and dose as factors) was performed separately for both beam qualities. P-values were adjusted for multiple testing using the false discovery rate (FDR) as described (Benjamini & Hochberg 1995). Genes were considered as being differentially expressed when the fold-change (FC) was 1.5≤ FC ≤-1.5 and FDR ≤0.05. Functional enrichment in the differential genes was studied using the ToppFun tool (http://toppgene.cchmc.org/) and applying an FDR corrected P-value of 0.05 for statistical significance. To further study the gene enrichment, the gene ontology tool GOrilla was used http://cbl-gorilla.cs.technion.ac.il/) with two un-ranked lists of genes (target and background gene lists) [3]. To test for the presence of differential gene expression after exposure of ECs to low or high LET radiation, a two-way ANOVA analysis with time and dose as factors was performed. Table 3 indicates the number of differentially expressed genes in comparison to the sham-irradiated samples of the same day. It can be seen that 0.05 Gy and 0.1 Gy of low LET radiation (Figure 2a) induces few transcriptional changes at 1 day after exposure. In contrast, higher doses (0.5 Gy and 2 Gy) of low LET radiation as well as low and high doses of high LET radiation (Figure 2b) induce a clear transcriptional response on day 1. Interestingly, only the 2 Gy dose of both low and high LET radiation induced a persistent difference in gene expression over the entire course of the experiments.

Table 3: Number of genes differentially expressed after exposure to low or high LET radiation (n=3)

▪ Applied dose	▪ 1 Day low LET	▪ 7 Days low LET	▪ 14 Days low LET	▪ 1 Day high LET	▪ 7 Day high LET
▪ 0.05 Gy	▪ 5	▪ 0	▪ 0	▪ 745	▪ 0
▪ 0.1 Gy	▪ 6	▪ 2	▪ 0	▪ n.d.	▪ n.d.
▪ 0.5 Gy	▪ 208	▪ 2	▪ 0	▪ n.d.	▪ n.d.
▪ 2 Gy	▪ 658	▪ 176	▪ 111	▪ 599	▪ 444

To study the underlying biology of the differentially expressed genes, hierarchical clustering was performed on 2000 genes with the most significant p-value for the time-dose interaction tested with two-way ANOVA. This method seeks clusters present in these 2000 genes that demonstrate comparable gene expression profiles over the different time and dose points. In order to identify potential molecular significance, the corresponding biological process and the cellular component of these individual clusters, gene ontology enrichment analysis was performed. Figure 2A demonstrates the outcome of the combined analysis for the low LET radiation genes. The angiogenesis-related processes, observed in cluster 1, were induced after exposure to 2 Gy of low LET radiation at the first day but were repressed after 1 week. Furthermore, the levels of genes involved in cell junctions and cellular adhesion (cluster 2) were changed two weeks after exposure to 2 Gy of low LET radiation. Next, the third cluster contains genes involved in the typical radiation-responsive pathways, e.g. the cell cycle progression, checkpoint control, DNA repair and recombination. The expression of genes of this cluster were repressed on the first day after 0.5 Gy and 2 Gy and induced in the first week after exposure to 2 Gy low LET irradiation. The fourth cluster, which constitutes genes, involved in the breakdown of macromolecules, show a differential response of the 2 Gy irradiated samples after 1 and 2 weeks. Figure 2B demonstrates the outcome of the combined analysis for the high LET radiation genes. From the heat maps in Figure 2 it can be seen that the induced effects on the transcriptional level are less pronounced at the low LET radiation than at the high LET radiation. The most prominent clusters (3, 4, 5 and 7) can be classified as typical radiation-responsive processes discussed in Figure 2A. In addition, cluster 2 contains genes involved in angiogenesis-related Wnt signalling. As can be seen from the heat map these genes were repressed 1 week after exposure to a high dose of Fe ions. Furthermore, clusters 3, 4 and 5 contain genes involved in poly(A)RNA binding. The differential expression of these genes at day 1 after exposure to 0.05 Gy Fe ions could indicate a fine-tuning of gene expression. A specific role for these genes could not be ascertained.

In order to study the differential response after high and low LET radiation exposure, lists of differentially expressed genes were compared at different doses and time points. Since this study did not include a high LET dose of 0.1 Gy and 0.5 Gy as well as the time point 14 days after exposure, these conditions were excluded from this part of the study. Figure 3A shows that 1 day after exposure to 0.05 Gy of Fe ions (green circle) and 0.05 Gy of X-rays (pink circle), 745 and 5 genes were differentially expressed, respectively. None of these genes were affected in both conditions. Gene ontology enrichment analysis indicated that the 745 genes that were affected by exposure to Fe ions were mainly involved in induction of DNA damage, p53 response and cell cycle changes. After high doses of high and low LET radiation, depicted in Figure 3B, there is more overlap between genes affected by both beam qualities: approximately half of the genes from either the low and high LET radiation group overlaps. Gene ontology enrichment of both the overlapping and the non-overlapping gene lists showed that they were all enriched in genes involved in i.e. DNA damage signalling, the p53 response and cell cycle changes. This indicates that both low and high dose LET radiation induce similar gene pathways to handle the radiation induced damage.

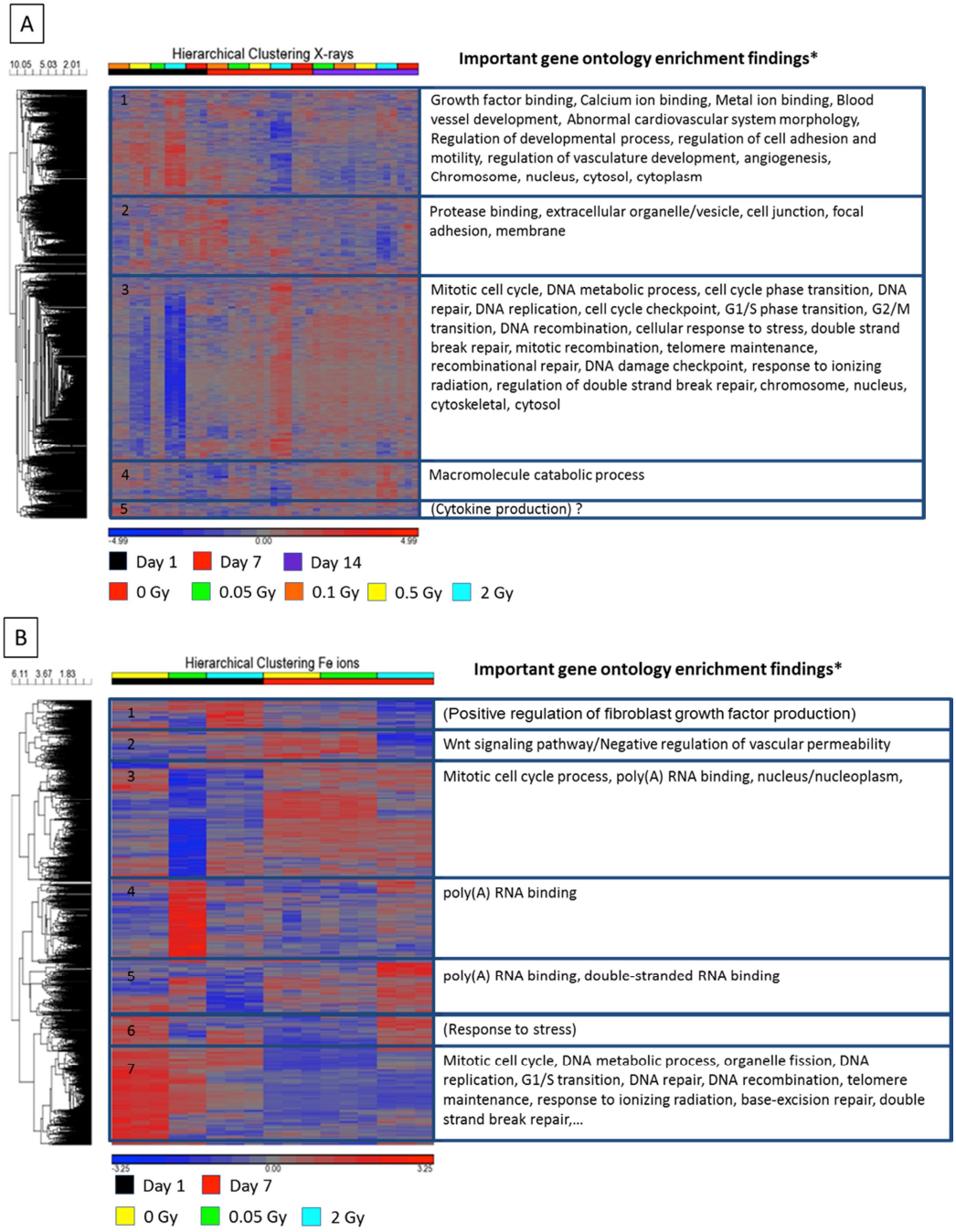

Figure 2: Hierarchical clustering and gene ontology enrichment of the 2000 top scoring genes for the low (A) and high (B) LET irradiated ECs. Ontologies between brackets demonstrated no FDR-corrected statistical relevance, but were assumed biologically significant. Blue, lowered gene expression; Red, increased gene expression.

Figure 3C indicates a reduced overlap at day 7 between the genes differentially expressed after exposure to 2 Gy of high and low LET radiation. While the genes affected by Fe ions play a role in angiogenesis, cytokine activity and cell cycle repression, the genes altered by X-rays are involved in the initiation of DNA replication and cell cycle progression. On the other hand, the overlapping genes at this time point indicate activity at the extracellular matrix with genes as von Willebrand Factor (vWF) being differentially expressed. Figure 3D represents a Venn diagram showing the overlap in differentially expressed genes after exposure to low dose Fe ions and high dose X-rays. Although both radiation qualities at these doses demonstrate a large overlap, many genes were altered by only one of the two forms of radiation. From gene ontology enrichment analysis it was found that the overlapping genes as well as the genes altered by a high X-ray dose are related to the typical response to ionizing radiation, e.g. cell cycle, DNA repair, chromosomal part and DNA replication. On the other hand, the

genes exclusively affected by a low dose of Fe ions represent diverse pathways which are not typically responsive to radiation such as cell adhesion, negative regulation of haemostasis and blood coagulation, negative regulation of wound healing and dipeptidyl-peptidase activity. These data indicate that the kinetics of the damage response is different for X-rays and Fe ions. Assuming that high LET irradiation is more efficient than low LET, we compared changes in gene expression induced by exposure to a high dose of low LET irradiation with those induced by a low dose of high LET irradiation.

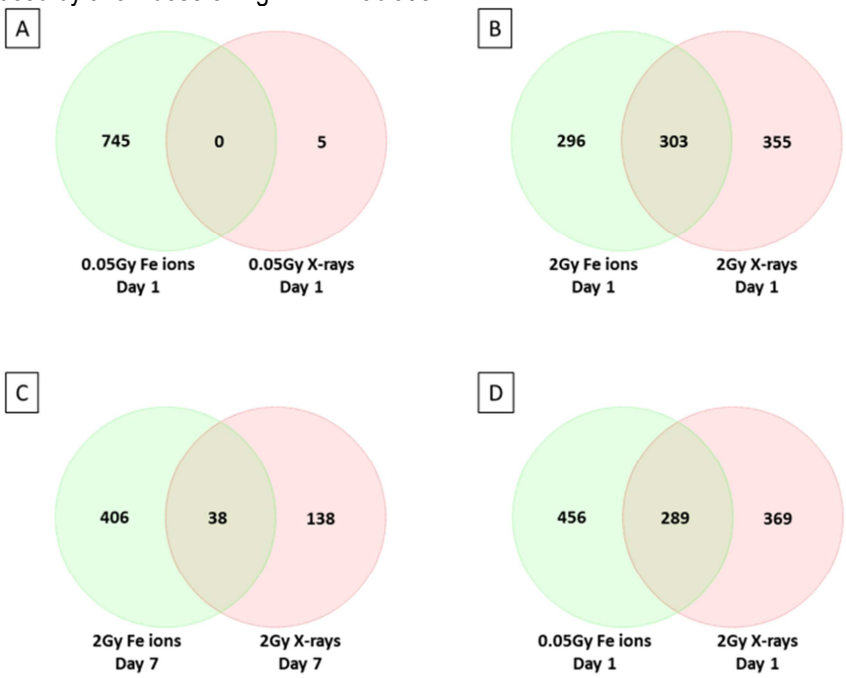

Figure 3 Overlap of significantly altered genes after irradiation with both radiation qualities.

1.3.2.2.2 Proteomic alterations after high and low LET irradiation

X-ray irradiation induced EC proteome alteration

Proteomics analysis of the EC 1 day after irradiation by 0.05 Gy and 2 Gy X ray showed that among quantified proteins 133 and 170 proteins were significantly differentially expressed in irradiated cells, respectively, compared to controls (+1.3-fold; $p<0.05$). 75 altered proteins were shared between the two doses. The number of significantly deregulated proteins showed a slight dose-dependent increase. The functional correlation analysis of the differentially expressed proteins was performed using GO categories with the PANTHER bioinformatics tool (http://www.pantherdb.org). Proteins with catalytic and structural molecular activity represented the largest group of molecular functions in all proteome profiles. A detailed analysis of the functional interactions and biological pathways was performed using the IPA software (http://www.INGENUITY.com). The analysis showed that the network “cell-to-cell signalling and interaction” was the most affected one in irradiated cells 24 hours post-exposure to both doses. IPA also showed that the pathways “cell adhesion and junction signalling”, and “caveolar-mediated endocytosis signalling” were significantly affected by 0.05 Gy and 2 Gy exposures after the first day.

Proteome profiling of the ECs seven days after irradiation using doses of 0.05 Gy and 2 Gy showed that 50 and 192 proteins were significantly differentially expressed in irradiated cells, respectively, compared to controls (+1.3-fold; $p<0.05$). 28 altered proteins were shared between two doses. The number of significantly deregulated proteins was markedly higher at the higher dose.

Differentially expressed proteins 7 days post-exposure were classified mainly as members of the networks “cell cycle and organ morphology” after exposure to 0.05 Gy and “cellular growth and proliferation” after exposure to 2 Gy. The pathways “gap junction signalling “and “caveolar-mediated endocytosis signalling” were still affected at this time point at both doses. The number of affected proteins involved in the cardiovascular system development and function was increased in a dose-dependent manner at this time point.

The canonical pathway analysis using both time points and doses showed that the number of deregulated proteins increased in a dose-dependent manner at both time points but the number of deregulated proteins decreased with time at the lower dose (0.05 Gy). The analysis confirmed alteration in the cell junction and adhesion (Table 4). Cell-cell adhesion and junction impairment are known as characteristic responses of the endothelium to increasing oxidative stress. The "caveolar endocytosis" pathway was affected at both doses and both time points suggesting an on-going pathological event (Table 5).

Fe-ions irradiation induced EC proteome changes

Proteomics analysis of the ECs 1 day after irradiation after doses of 0.05 Gy and 2 Gy using Fe-ions showed that 176 and 325 proteins were significantly differentially expressed in irradiated cells, respectively, compared to controls (+1.3-fold; $p<0.05$). 35 altered proteins were shared between the two doses. The number of deregulated proteins significantly increased after Fe-ion exposure compared to X-ray exposure using the same dose, suggesting more pronounced changes after heavy ion irradiation. The number of significantly deregulated proteins was increased in a dose-dependent manner. The functional correlation analysis of the differentially expressed proteins was performed using GO categories with the PANTHER bioinformatics tool (http://www.pantherdb.org). Molecular functions "metabolism" and "cytoskeletal organisation" had the largest number of deregulated proteins in all proteome profiles. More detailed analysis of the functional interactions and biological pathways was performed using the IPA software (http://www.INGENUITY.com). IPA showed that the pathways "cell adhesion junction" and "protein ubiquitination" were significantly affected at 0.05 Gy and 2 Gy exposures, respectively, after the first day.

Proteome profiling of the EC seven days after Fe-irradiation at 0.05 Gy and 2 Gy showed that 208 and 307 proteins were significantly differentially expressed in irradiated cells, respectively, compared to controls (+1.3-fold; $p<0.05$). 64 altered proteins were shared between two doses. The number of significantly deregulated proteins increased with time suggesting a progressing and persistent cellular damage.

Differentially expressed proteins 7 days post-exposure were classified mainly as members of the networks "cellular assembly and organisation" after exposure to 0.05 Gy and "cellular growth and proliferation" after exposure to 2 Gy. The analysis suggested that pathways "caveolar endocytosis "and "integrin signalling" were activated after both 0.05 Gy and 2 Gy.

X-ray radiation-induced SMC proteome alteration

Proteomic analysis of the SMC 24 hours after irradiation by 0.05 Gy and 2 Gy showed that 68 and 119 proteins were significantly differentially expressed in irradiated cells, respectively, compared to controls (+1.3-fold; $p<0.05$). 26 altered proteins were shared between the two doses. The number of deregulated proteins showed a dose-dependent increase after the first day.

The functional correlation analysis of the differentially expressed proteins was performed using GO categories with the PANTHER bioinformatics tool. It indicated that the proteins involved in the catalytic and structural organisation activity represented the most important molecular functions in all proteome profiles. Functional interaction and biological pathway analysis was performed using the IPA software. The analysis showed that the most important networks were "cell-to-cell signalling and interaction and cell morphology" (0.05 Gy) and "lipid and protein metabolism" (2 Gy) after day 1. IPA indicated additionally that the pathways "glycolysis" and "actin cytoskeleton signalling" were significantly affected after the first day using X-ray doses of 0.05 Gy and 2 Gy, respectively.

Proteome profiling of the SMC 7 days after irradiation by 0.05 Gy and 2 Gy showed that 172 and 108 proteins were significantly differentially expressed in irradiated cells, respectively, compared to controls (+1.3-fold; $p<0.05$). 53 altered proteins were shared between the two doses. Interestingly, the direction of the deregulated proteins was in the majority of cases opposite at low vs. high dose resulting for example in inactivation of integrin/paxillin pathway at 0.05 Gy but activation at 2.0 Gy. Still, the majority of differentially expressed proteins were members of the network "cell morphology" at both doses. The analysis showed a consistent alteration in the actin cytoskeleton signalling and calcium transport. Both processes are involved in the muscle contraction.

Fe-ion radiation-induced SMC proteome changes

Proteomics analysis of the SMC 1 day after irradiation by 0.05 Gy and 2 Gy Fe-ions showed that 287 and 374 proteins were significantly differentially expressed in irradiated cells, respectively, compared to controls (+1.3-fold; $p<0.05$). 178 altered proteins were shared between the two doses. The number of significantly deregulated proteins was increased in a dose-dependent manner. The functional correlation analysis of the differentially expressed proteins was performed using GO categories with the PANTHER bioinformatics tool (http://www.pantherdb.org). "Metabolism" and "structural proteins" were the most important molecular functions in all proteome profiles. More detailed analysis of the functional interactions and biological pathways was performed using the IPA software. IPA showed that "EIF2 signalling", and "actin cytoskeleton" were significantly affected by 0.05 Gy and 2 Gy exposures after the first day. Proteome profiling of the SMC seven days after Fe irradiation by 0.05 Gy and 2 Gy showed that 161 and 308 proteins were significantly differentially expressed in irradiated cells, respectively, compared to controls (+1.3-fold; $p<0.05$). 76 altered proteins were shared between two doses. Differentially expressed proteins 7 days post exposure were classified mainly as members of the networks "skeletal and muscular disorder" after exposure to 0.05 Gy and "cellular assembly and organisation" after exposure to 2 Gy. The pathways "actin cytoskeleton" and "integrin signalling" were affected at both doses. The number of deregulated proteins significantly increased after Fe-ions exposure compared to X-ray exposure, suggesting more pronounced changes after heavy ion irradiation.

Production and release of cytokines after high and low LET exposures

The cytokine release was performed by GSI using bead based protein arrays. After irradiation, medium supernatants were collected at the indicated time points and frozen at -80°C. Medium was replaced 24 h before each time point. The concentrations of inflammation related cytokines in the supernatants of mono- and cultures were determined by bead-based protein arrays (eBioscience, BectonDickenson). Based on these results, concentrations of selected cytokines were quantified using ELISA (eBioscience). Measured concentrations were normalized on the cell numbers/ml supernatant and calculated as the fold change compared to the control cells of the respective time point. The results of selected cytokines were validated by ELISA (IL-6, IL-8, MCP-1). TGF-β1 concentrations were quantified using ELISA (eBioscience). The putative relationship to an inflammatory response in heart (Testa et al. 1996) was carried using a bead based cytokine array. To confirm the results obtained previously we repeated experiments to obtain results from 1 (Fe ions) or 2-3 (X-ray) independent experiments, measured in duplicates or triplicates. The compiled results are shown in Figure 4. In 2 X-ray experiments, the variation of the measured cytokine concentrations was high, therefore most of the changes were trends and the level of significance was > 0.05. reason was most likely due to one centrifugation step in the working flow, which reduced the robustness of the method. In a next step, the release of cytokines by EC and SMC after X-ray exposure was validated by ELISA. For X-ray exposure, 2-3 independent experiments were performed (duplicates or triplicates), whereas due to limited availability of beam time a pilot experiment was carried out using Fe ions. Interleukin-6 (Gallo et al. 1997) plays a major role in inflammatory processes and is released by many cell types.

Table 4. Significantly deregulated proteins involved in the cell adhesion and junction in ECs. The up-regulated proteins are marked in red and the down-regulated in green.

	proteins involved in the cell adhesion and junction	Fold Change	Fold Change	Fold Change	Fold Change	Fold Change	Fold Change	Fold Change	Fold Change
Symbol	Entrez Gene Name	50 mGy Xray 24h	50 mGy Fe 24h	50 mGy X ray 1W	50 mGy Fe 1W	2Gy Xray 24h	2Gy Fe 24h	2Gy X ray 1W	2Gy Fe 1W
ACTC1	actin, alpha, cardiac muscle 1		1.3				1.6		
ACTN4	actinin, alpha 4		1.4			1.3			
CAV1	caveolin 1, caveolae protein, 22kDa			-1.3	1.6	-1.7		-1.8	1.6
CTNNA1	catenin alpha 1		1.3		1.3		1.3		
CTNNB1	catenin beta 1	1.5		1.5	1.3	2.2		2.7	2
F11R	F11 receptor				1.5				1.6
ILK	integrin-linked kinase				-1.5				
ITGA2	integrin, alpha 2				1.8	1.3		-1.5	2.6
ITGA3	integrin, alpha 3								1.3
ITGA5	integrin, alpha 5					1.4		1.3	1.9
ITGB1	integrin, beta 1				1.4				1.5
JUP	junction plakoglobin					1.3			
MAPK1	mitogen-activated protein kinase 1		1.3						
NOS3	nitric oxide synthase 3 (endothelial cell)	1.3				1.3			
NRAS	neuroblastoma RAS viral (v-ras) oncogene homolog				1.4				1.3
PRKAR2B	protein kinase beta				-1.6				
RRAS	related RAS viral (r-ras) oncogene homolog			-1.3	1.5			-1.4	4.5
RRAS2	related RAS viral (r-ras) oncogene homolog 2				1.3				1.4
SPTAN1	spectrin, alpha, non-erythrocytic 1	1.4	1.3			1.6	1.4		
SPTBN1	spectrin, beta, non-erythrocytic 1	1.6				1.4			
SPTBN1	spectrin, beta, non-erythrocytic 1	1.6				1.4			
TJP1	tight junction protein 1				1.3	1.5			
TJP2	tight junction protein 2	1.3							
TUBA4A	tubulin, alpha 4a				-1.3	1.3	1.3	1.4	
TUBB	tubulin, beta class I				-1.4			1.3	
TUBB6	tubulin, beta 6 class V				-1.3		1.3	1.5	

Table 5. Significantly deregulated proteins involved in caveolar-mediated endocytosis signalling in EC. Up-regulated proteins are marked in red and the down-regulated in green.

	proteins involved in the caveolar-mediated endocytosis	Fold Change	Fold Change	Fold Change	Fold Change	Fold Change	Fold Change	Fold Change	Fold Change
Gene ID	Gene Name	50 mGy Xray 24h	50 mGy Fe 24h	50 mGy X ray 1W	50 mGy Fe 1W	2Gy Xray 24h	2Gy Fe 24h	2Gy X ray 1W	2Gy Fe 1W
ACTC1	actin, alpha, cardiac muscle 1		1.3						
ALB	albumin		2.6						
B2M	beta-2-microglobulin							1.3	
CAV1	caveolin 1, caveolae protein, 22kDa			-1.3	1.6	-1.7		-1.8	1.6
COPB1	coatomer protein complex, subunit beta 1		1.4						
COPB2	coatomer protein complex, subunit beta 2	-1.3							
COPE	coatomer protein complex, subunit epsilon				-2.3				-2.3
COPE	coatomer protein complex, subunit epsilon								
COPG1	coatomer protein complex, subunit gamma 1						1.3		1.4
DNM2	dynamin 2				-1.5				
FLNA	filamin A, alpha	-1.3			-1.6				
FLNB	filamin B, beta				-1.4				-1.332
FLNC	filamin C, gamma					1.7	1.4		
FLOT1	flotillin 1							-1.6	
FLOT2	flotillin 2					-1.5		-1.8	
HLA-A	major histocompatibility complex, class I, A				1.4				1.6
HLA-B	major histocompatibility complex, class I, B				1.4				1.7
HLA-C	major histocompatibility complex, class I, C				1.8				2.5
ITGA2	integrin, alpha 2				1.8	1.3		-1.5	2.6
ITGA3	integrin, alpha 3								1.269
ITGA5	integrin, alpha 5					1.4		1.3	1.9
ITGAV	integrin, alpha V	1.3			1.7				
ITGAV	integrin, alpha V					1.3			1.5
ITGB1	integrin, beta 1				1.4				1.5
ITGB5	integrin, beta 5				2.6				
PTRF	polymerase I and transcript release factor				-1.6				-1.6
RAB5A	RAB5A, member RAS oncogene family				1.4				1.4
RAB5C	RAB5C, member RAS oncogene family					-1.3		-1.8	1.3

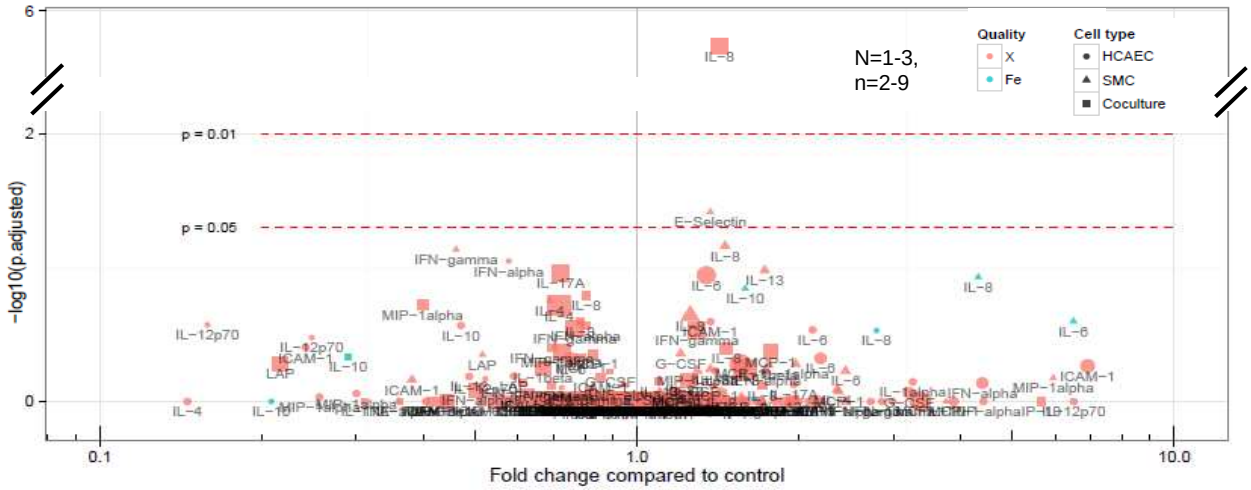

Figure 4: Changes in cytokine release compared to control cells after irradiation with X-rays (X) or 1 GeV/u Fe ions (Fe) for EC, SMC and the co-culture, assessed by bead based arrays.

Cytokine release and adhesion after high and low LET irradiation

The first step of selection of the cytokines, which are changed after irradiation and have a known or The The radiation induced changes of IL-6 release in EC are shown for 1 week after exposure to X-rays and Fe ions in Figure 4 the other time points which were investigated did not show significant changes (4h, 24h, 2 weeks). One week after X-ray irradiation, we observed in EC and in the co-culture a dose dependent increase of IL-6 release. In SMC no elevated levels of IL-6 were measured. Notably, no specific effect at low doses could be detected, i.e. no significant changes were observed for doses ≤ 0.5 Gy (EC) und for doses < 0.5 Gy (co-culture) do not show a significant change. In contrast, one week after Fe ion irradiation, we measured an up to twofold increase of IL-6 release at the low dose measured (0.05Gy) in ECs and in the co-culture, as a trend also in SMCs. After exposure to the high dose (2Gy) IL-6 levels were less elevated compared to the low dose exposure (EC) or not elevated compared to control cells (SMC, co-culture).

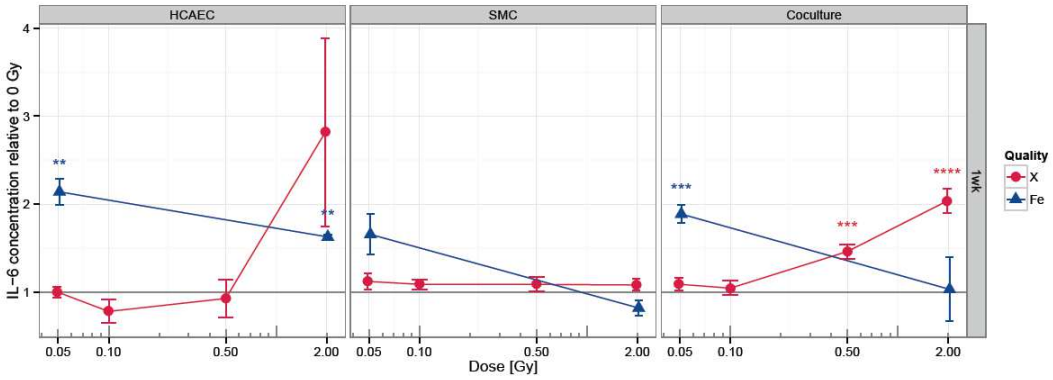

Figure 5: IL-6 release of EC, SMC and the co-culture one week after exposure to X-rays or 1 GeV/u Fe ions.

Interleukin-8 (IL-8) has an influence on the proliferation of ECs and acts as a chaemoattractant. As enhanced adhesion is one step in the inflammatory process and it was clearly enhanced after irradiation in the bead based array measurements, we investigated the release of IL-8 after radiation exposure. The radiation induced changes of IL-8 release in EC are very similar to IL-6,. One week after X-ray irradiation, we observed in EC and in the co-culture a dose dependent increase of IL-8 release. In SMC no elevated levels of IL-8 were measured. No specific effect at low doses could be detected for EC (for doses ≤ 0.5 Gy), whereas the measured values of the co-culture indicate a small enhancement already for 0.05Gy, although the biological relevance of such a small change has to be critically considered. Again similar to IL-6, one week after Fe ion irradiation, we measured an up to 2.5fold increase of IL-8 release at the low dose measured (0.05Gy) in EC and in the co-culture, but unlike IL6 this cytokine was also released by SMC.

Adhesion to irradiated EC was increased one week after irradiation at high, but not at low X-ray doses (see Figure 12 for details). Other time points tested did not show significant changes (4h, 24h), or the dose response was unclear.

Exposure to Fe ions resulted in a reduction of adhesion compared to controls, in contrast to X-ray exposure not only for the high but also for the low dose (Figure 12). Unexpectedly, the cytokine release for IL-6, IL-8 and MCP-1 was increased, suggesting that additional (cytotoxic) factors, operating after Fe ion but not after X-ray exposure, influence the functional behaviour.

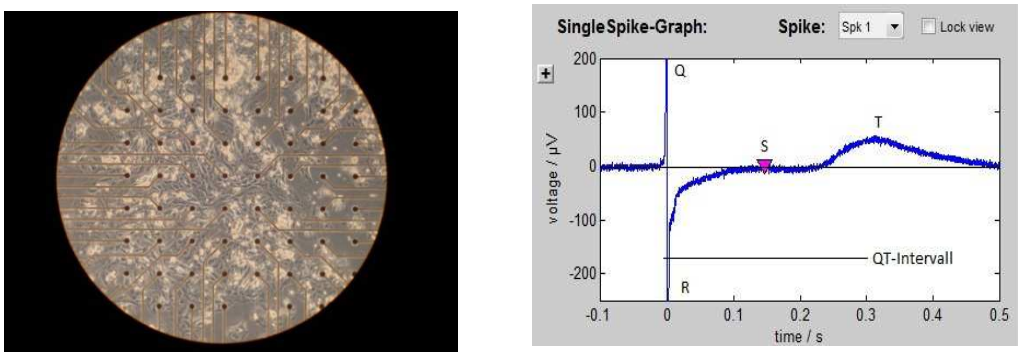

Figure 6: Electrophysiological analysis of cardiomyocytes derived from embryonic stem cell using MEA technology. Left: Cardiomyocytes cultured on a MEA chip. Right: Representative recording

Electrophysiological changes after high and low LET irradiation

Cardiomyocytes derived from mouse embryonic stem cells (Wobus & Löser 2011) were used to examine the impact of low LET X-rays and high LET C-ions on electrophysiology up to 7 days post-irradiation.

The MEA micro electrode array technology (Multi Channel Systems, Germany) was used for the non-invasive extracellular recording of endpoints such as beat-rate, field action potential duration (fAPd, field action potential duration. We used commercially available Cor.At cells. There pure primary-like cardiomyocytes seeded on fibronectin-coated MEAs (Axiogenesis, Germany). Preceding studies using patch clamp analyses and MEA recordings have already demonstrated the normal electrophysiological properties of these cells [2] (Figure 6). Radiation exposure was performed two days after seeding when cells had built up a beating network. Cells were irradiated with either C-ions (spread-out Bragg peak, twelve energies ranging from 107-147 MeV/u, mean LET = 70 keV/µm at target position) accelerated at the SIS18 or 250 kV X-rays (250 kV, 16 mA). The doses used for both radiation qualities were 0.5 and 2 Gy. The first recordings were performed a few hours before exposure. Then, measurements were conducted at 24h intervals post-irradiation for up to seven days. Having established the experimental set up as sound we studied the impact of 0.5 and 2 Gy X-rays or C-ions on the electrophysiology of cardiomyocytes up to 1 week post-irradiation. In total 139 samples (i.e. MEAs) were analysed and no dose- or radiation quality dependent change of the beat rate was observed in comparison to the respective controls. Likewise, fAPd, minimum and maximum of the signal amplitude, conduction velocity and number of active electrodes showed no radiation-induced alterations.

3.3 Dose rate effects

3.3.1 Comparing chronic and acute exposures on atherosclerosis

3.3.1.1 Effects of chronic irradiation on atherosclerosis

It is currently standard practice to assume that the risk of cancer is less when the dose is applied in a protracted or fractionated manner, rather than as an acute dose. A dose rate correction factor is applied to take account of this for low dose rate exposures. With our partner, the Institute of Ecological Sciences, Rokkasho, Japan, we have compared the effects of extremely low dose rates with those of the same doses delivered acutely. At IES a total of 126 female C57BL/6 ApoE$^{-/-}$ mice (42 per group) were randomly assigned to three irradiation groups: (1) 20 mGy/day for 15 days (total accumulated dose of 0.3 Gy); (2) 20 mGy/day for 300 days (total accumulated dose of 6 Gy); and, (3) 1 mGy/day for 300 days (total accumulated dose of 0.3 Gy). An additional 84 mice were assigned to two non-irradiated control groups of 42 mice each for the 15- and 300-day groups. Due to space constraints in the irradiation rooms, two sets of experimental groups were generated and exposed. A total of 126 female C57BL/6 ApoE$^{-/-}$ mice (42 per group) received acute irradiation at ENEA with single doses of 0.3 or 6 Gy X-rays at a dose rate of 0.89 Gy/min.

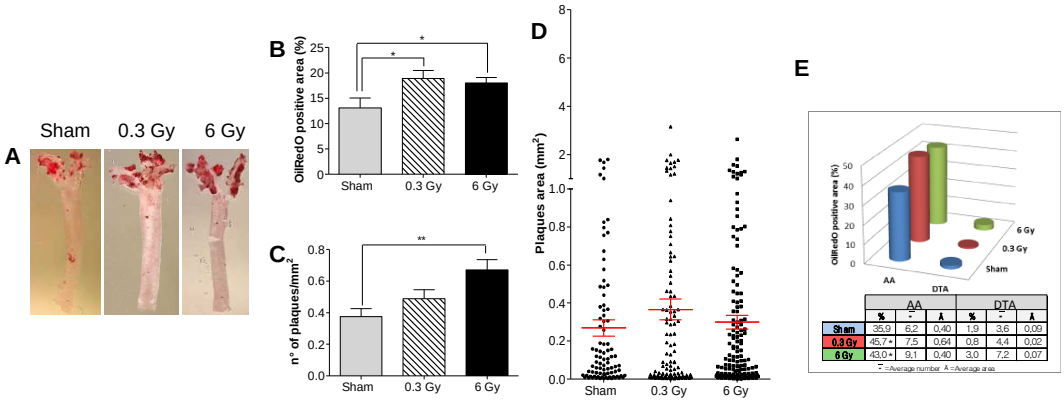

Figure 7 Acute irradiation. (A) Representative *en face* preparations of aortas from female ApoE$^{-/-}$ mice 300 days after acute exposure to 0.3 Gy, 6 Gy and from age-matched controls. (B-D) Morphometric analyses on digital images from *en face* preparations of aortas (n=8) representing percentage of ORO-stained area (B), plaques density (C) and plaques size (D). (E) Regional distribution of plaques.

Mice were euthanized 300 days (0.3 and 6 Gy) or 15 days (0.3 Gy) after exposure. Controls (n=84, 42 per time point) were sham acute irradiated. Hearts and thoracic aortas were collected from irradiated and sham-irradiated mice for plaque morphometry, and for histological and immunohistochemical analysis. For quantitative analysis of plaque area and number, dimensional analysis of digital images from *en face* Oil-Red-O (ORO)-stained thoracic aortas was carried out (Figure 7A). The mean percentage of plaque-covered aorta area was significantly increased at 300 days from acute exposure to both X-ray doses compared with sham-irradiated mice (Figure 7B; P<0.05). Two different factors, number of plaques and their size, can contribute alone or in combination to the increased amount of lipid-laden area in irradiated ApoE$^{-/-}$ mice. Irradiation at all doses caused a general increase in density of atherosclerotic lesions (# of plaques/mm^2) (Figure 7C). Indeed, in mice irradiated with 0.3 Gy, a combination of non-statistical increases in density (1.3-fold; *P*=0.1501) and plaque size (Figure 7D; 0.36 ± 0.054 *vs* 0.26 ± 0.042) resulted in a statistical increase in terms of ORO-stained total area (Figure 7C). At 6 Gy the density of atherosclerotic lesions increased significantly (1.8-fold; *P*= 0.0022), while plaque size remained very similar to that measured in sham-irradiated mice (Figure 7D; 0.29 ± 0.036 *vs* 0.26 ± 0.042). Atherosclerotic plaques developed principally in the aortic arch (AA), a region presenting both a high curvature zone and bifurcations. Figure 7E shows the regional distribution of ORO-stained plaques in sham-irradiated ApoE$^{-/-}$ mice, with lesions located predominantly in the AA region (35.9%) and rare plaques in the descending thoracic aorta (DTA) (1.9%). A similar regional distribution was observed after irradiation. However, the lipid-laden area in the AA increased with irradiation. In fact, mice exposed to 0.3 Gy showed a 1.6-fold increase in plaque area in the AA (45.7%) although there was no variation in plaque number. In contrast, mice irradiated with 6 Gy showed a 1.5-fold increase in number of AA plaques and no size variation (43.0%). Mice irradiated with 6 Gy showed presence of plaques in the DTA region (3.0%), although the increase in their number was not significant. Altogether, these results show that an acute dose of radiation increases atherogenesis in ApoE$^{-/-}$ mice, suggesting that the mechanisms for plaque formation is different between low and high doses of radiation, acting as plaque promoting or initiating stimulus, respectively.

The spontaneous level of atherosclerotic lesions in 360-days old ApoE$^{-/-}$ mice at the IES animal facility, was 4-fold higher than that observed in the age-matched ApoE$^{-/-}$ mice housed at ENEA (44.8% *vs* 11.3%; *P*<0.0001). The baseline regional distribution of plaques was also very different. Because mice were purchased from the same producer and belonged to the same batch, and fed the same diet, we hypothesize that different housing conditions (SPF *vs* conventional) strongly influenced atherosclerosis. Despite baseline differences, comparison of atherogenic radiation responses in the two colonies yields useful information

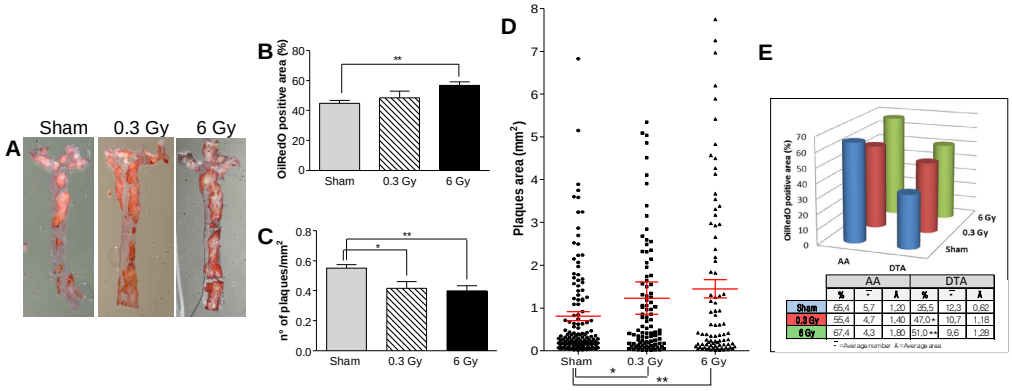

Figure 8 Chronic irradiation. (A) Representative ORO-stained aortas from female ApoE$^{-/-}$ mice after chronic irradiation with 0.3 Gy or 6 Gy over 300 days, and age-matched controls. Graphic representation of quantitative analyses performed on digital images from en face preparations of aortas (n=8) showing: (B) the percentage of ORO-stained aortic area; (C) plaque density; (D) plaques size and their regional distribution (E).

After chronic irradiation, the mean percentage of thoracic aorta area covered by plaque was significantly increased, compared with controls, only in mice exposed to 6 Gy (Figure 8A and 8B; *P*=0.002). Although the density of plaques showed significant decrease both after 0.3 Gy (0.55 ± 0.02 *vs* 0.41 ± 0.04; *P*=0.0318) and 6 Gy (0.39 ± 0.03; *P*=0.0024), compared with controls (Fig 2C), the mean plaque area was significantly higher in both groups, which for the 6-Gy dose resulted in significant overall increase. A 1.5- (*P*=0.0401) and 1.8-fold (*P*=0.0034) increase in plaque area was quantified in 0.3- and 6-Gy irradiated mice, respectively, over controls (Figure 8D), which suggests coalescence of existing or de novo plaques resulting in apparent decrease in frequency (Figure 8C). Regional distribution analysis of plaques (Figure 8E) showed a high percentage of AA area covered by plaques in control mice (65.4%). The DTA region also showed dramatic involvement in the atherogenic process (35.5%). Because of massive presence of plaques in the AA, the effect induced by chronic irradiation was assessed as percentage of ORO-stained area in the DTA. As shown in Fig 2E, chronic irradiation significantly increased the mean percentage of DTA covered by plaques after both 0.3 and 6 Gy (47% and 51%, respectively). This global increase was due to 1.9-fold and 2.0-fold increases in plaque size in 0.3 Gy- (*P*=0.0205) and 6 Gy-irradiated mice (*P*=0.0064), respectively, relative to controls.

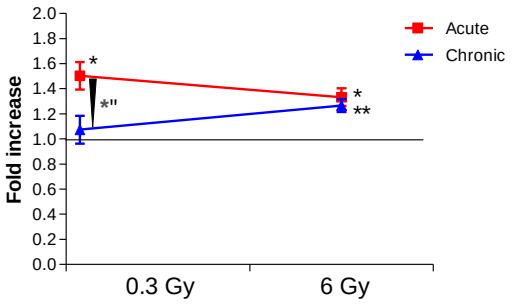

Figure 9 Comparison of fold increases of ORO-stained aortic area over sham-irradiated controls between high and low dose-rate groups.

3.3.1.2 Acute versus chronic irradiation on atherosclerosis

Although direct comparisons of the extent of atherogenesis between high and low dose-rate groups cannot be made, results have been interpreted based on the fold increase in atherosclerosis (%ORO-stained area) in irradiated compared to sham-irradiated groups. A high radiation dose (6 Gy) was equally efficient in promoting atherogenesis at

both high and low dose rate (Figure 9), whereas a moderate dose (0.3 Gy) could significantly enhance atherogenesis only if delivered acutely (*P*=0.0143, acute *vs.* sham irradiated). By comparing fold increases, mice receiving 0.3 Gy acutely showed enhanced atherogenesis compared with mice receiving the same dose as a chronic exposure (*P*=0.0298). A similar dose-rate effect was not detected at 6 Gy (Figure 9).

3.3.3 Phenotypic analysis of mouse hearts exposed to different dose rates using proteomic

At HMGU, the changes in the total cardiac proteome of acute and chronically irradiated ApoE $^{-/-}$ female mice were analysed with quantitative proteomics by using ICPL duplex platform. Bioinformatics tools such as Ingenuity Pathway Analysis (IPA) and STRING were used for visualization of protein networks and prediction of upstream targets.

Acute effects on the proteome

Twenty proteins after 15 days (0.3 Gy), 11 proteins after 300 days (0.3 Gy) and 23 proteins after 300 days (6 Gy) were found significantly deregulated. The lack of shared deregulated proteins between the two time points suggested that the proteomic response is distinct at each time. The early response (15 days, 0.3 Gy) may be considered as a typical "shock-like" response but had disappeared after 300 days (0.3 Gy) to be replaced by markers linked to heart disease.

Chronic low-dose-rate effects on the proteome

After 0.3 Gy given in 15 days (dose rate 20 mGy/d), only 6 significantly changed proteins in the cardiac proteome of ApoE-/- mice were observed. The long-term effects (300 days) with the accumulated dose of 0.3 Gy (dose rate 1 mGy/d) showed 13 proteins significantly changed. Using the higher dose rate during 300 days (accumulated dose 6.0 Gy) resulted in 24 cardiac proteins significantly deregulated, as with the response to the 6 Gy acute, typical markers of cardiac disease were deregulated at this dose.

Acute vs. chronic exposure: comparison

There were only two deregulated proteins that were common at high acute and chronic doses: annexin A6 and aldehyde dehydrogenase 2. "Oxidative phosphorylation" was the first hit in the comparison analysis of significantly changed proteins at 300 days post-irradiation. Proteins belonging to the category "Fatty acid beta oxidation" were found affected only at acute doses.

3.3.4 Phenotypic analysis of mouse hearts exposed to different dose rates using transcriptomics

Microarray (Affymetrix) analysis was performed by SCK•CEN with total RNA of lysed dissected irradiated mouse hearts (biological triplicates for each condition) (1,2). Data analysis was performed using Partek Genomics Suite v6.6 software via a three-way ANOVA analysis with dose rate (acute vs. chronic), time (15 vs. 300 days) and dose (0, 0.3 and 6 Gy) as factors (Fig xxx). In order to identify enriched gene ontology (GO) terms within the microarray dataset GOrilla (Gene Ontology enRIchment anaLysis and visuaLizAtion tool) was used. Data are being validated by RTqPCR.

Effect of acute exposure on the transcriptome

After acute exposure, 52 (0.3Gy-15d), 268 (0.3 Gy-300d) and 512 (6Gy-300d) differentially expressed genes were identified *vs.* sham-irradiated samplesThus, the number of differentially expressed genes increased with radiation dose (comparison at 300 days) and time of sampling after irradiation. There was not much overlap in terms of numbers of differentially expressed genes between 15 and 300 days sampling after exposure (0.3Gy-15d *vs.* 0.3Gy-300d: 2 genes; 0.3Gy-15d *vs.* 6Gy-300d: 2 genes). In contrast, substantial overlap was observed for samples analysed 300 days after irradiation with 0.3 or 6 Gy (0.3Gy-300d *vs.* 6Gy-300d: 95 genes). Not many GO terms were found for the acute 0.3 Gy 15 day samples. For the acute 0.3 Gy 300 days samples there are GO terms linked to cell growth, inflammation, and cell surface/extracellular region, which all three could be a sign of a pro-atherosclerotic state. GO terms for the acute 6 Gy 300 days samples are mainly linked with transcription. The intersection of acute 0.3 Gy and 6 Gy 300 day samples contains Go terms regarding inflammation, nucleoside catabolism, and ion channel activity.

Effect of chronic exposure on the transcriptome

After chronic exposure, 235 (0.3Gy-15d), 140 (0.3Gy-300d) were identified. The number of differentially expressed genes increased with the total dose (comparison at 300 days, no data for 6 Gy-15 days). For a total chronic dose of

0.3 Gy, there were more genes differentially expressed using a higher dose rate (20 mGy/day over 15 days) compared to a lower dose rate (1 mGy/day over 300 days). Similar to acute exposure, there was not much overlap in terms of numbers of differentially expressed genes between 15 and 300d groups (0.3 Gy-15 days *vs.* 0.3 Gy-300 days: 1 gene; 0.3 Gy-15 days *vs.* 6 Gy-300 days: 4 genes). There was more overlap for samples analysed 300 days after irradiation with 0.3 or 6 Gy (0.3Gy-300 days vs. 6 Gy-300 days: 32 genes). While the chronic 0.3Gy-15d samples showed a substantial amount of differentially expressed genes *vs.* sham-irradiated-15d samples, not many GO terms were found. Also, for the chronic 0.3Gy-300d samples, the list of relevant GO terms is limited to regulation of proteolysis. GO terms of the chronic 6 Gy-300d samples are linked with phosphatidylinositol-3-kinase signalling, (vascular) development, and cell motility. GO terms for the intersection of chronic 0.3 Gy and 6 Gy 300d samples are limited to the regulation of DNA biosynthetic processes.

Comparing acute vs. chronic exposure

In 0.3Gy-15d groups, more genes were differentially expressed *vs.* sham-irradiated samples after chronic dose compared to acute exposure. In 300d groups, however, more genes were differentially expressed after acute compared to chronic exposure to 0.3 or 6 Gy. For both acute and chronic exposure, the number of differentially expressed genes increased with dose. Although substantial overlap was seen after 300 days between doses for both dose rates, there was not much overlap between acute and chronic irradiated samples for both time points (0.3Gy chronic-15d vs. 0.3Gy acute-15d: 1 gene; 0.3Gy chronic 300d *vs.* 0.3Gy acute 300d: 10 genes; 6Gy chronic 300d vs. 6Gy acute 300d: 7 genes). Cell-cell interaction, Want/Notch signalling and insulin-related processes for both the acute and chronic irradiation was identified. Overlap between different doses and dose rates at 300 days were minimal.

Collection and analysis of heart tissue from SUBI Radiobiological Repository of Human Tissues

The identification of biological samples suitable for proteomic analysis was carried out by SUBI. Criteria for inclusion or exclusion from the study were agreed beforehand. Samples were divided into 3 groups depending on the total dose of external gamma rays, i.e. <100 mGy, 100-500 mGy and >500 mGy. In all, 67 archival samples of the left ventricle from individuals eligible for inclusion and for who at least 2 paraffin blocks with left ventricle tissue were available. A total of 62 blocks were received by HMGU and used to isolate RNA for microRNA (miRNA) analysis. miRNA expression changes were detected by low-density array analysis and differences were analysed in view of the miRNAs role in cardiovascular diseases with emphasis on their implication in the inflammatory processes that accompany heart failure, atherosclerosis, and coronary artery disease.

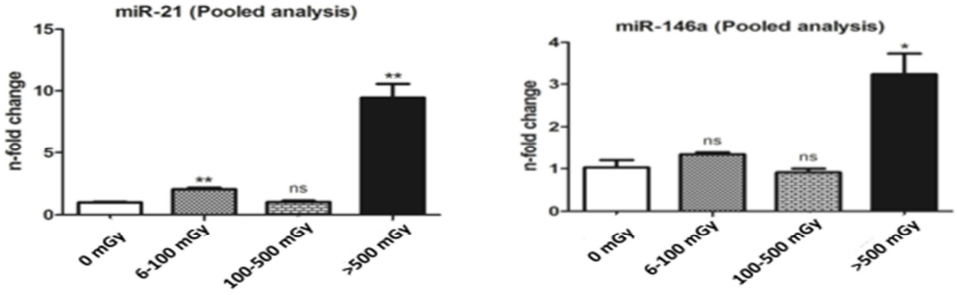

Figure 10 miRNA differential expression using specific single miRNA assays. A) miR-21, B) miR-146a. Significance is marked with asterisks *<0.05 and **p< 0.001.

3.4 Cell-cell interactions and their contribution to cardiovascular risk

3.4.1 Abscopal effects of radiation on the vasculature

To investigate abscopal effects of radiation on the vasculature, at the ENEA, long-range radiation effects have been investigated in vivo using ApoE$^{-/-}$ hyperlipidaemic mice prone to the development of atherosclerotic plaques. Cohorts of these mice were irradiated at the age of 8 weeks with X-rays at doses of 0, 0.05, 0.1 and 2 Gy, using custom-built lead shields that allow complete protection of the heart, thorax, and kidneys, while exposing the remaining parts of the mouse body. Shielding was checked by dosimetry and Monte Carlo simulation, and a conservative value of the dose (attenuated + scattered) of 1.4% of the total dose to shielded tissues was estimated. Groups of 10 mice per dose and time point were exposed and examined for the development of plaques. Animals were sacrificed at the age of 20 and 60 weeks. Irradiated mice were examined in histological and molecular studies and compared to control

ApoE$^{-/-}$ cohorts. For quantitative and morphometric analyses of atherosclerotic plaques, thoracic aortas were dissected and briefly fixed in 10% neutral buffered formalin. After removal of any adventitial fat, aortas were cut longitudinally, pinned en face on wax foils and stained with 1.8% Oil-Red.

At all doses, analysis was restricted to the aortic arch region, due to low numbers of plaques in the descending thoracic aorta. The results in Figure 11 show that no effects were observed on the percentage of oil-Red-ORO-stained lipid-laden areas of mice exposed to low doses (i.e., 0.05 and 0.1 Gy) at either 20 or 60 weeks of age, suggesting that long-range tissue interactions leading to increased or decreased atherogenesis are not produced by low radiation doses. The mean plaque area was significantly higher after a 2Gy exposure, indicating acceleration of atherogenesis of long-range tissue after exposure to a moderate dose of radiation. This acceleration of early-stage lesion area lost statistical significance as time progressed, and it was barely evident when the mice were examined at 60 weeks of age, presumably as the aorta becomes filled with plaques. This result suggests that 2 Gy doses to the periphery may increase atherosclerotic plaque formation at an early age.

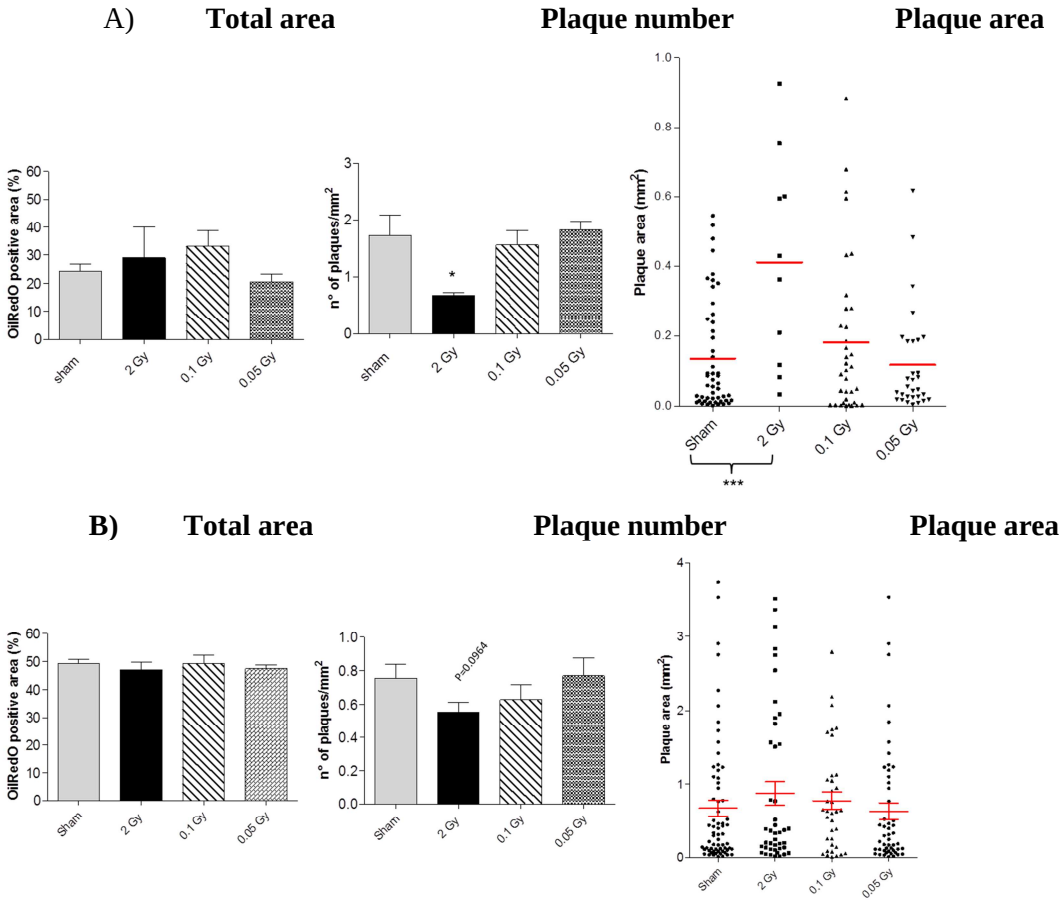

Figure 11: Quantification of plaque area and number in aortic arch of ApoE-/- mice A) 20 weeks or B) 60 weeks following non-cardiac irradiation.

3.4.2 Role of mast cells in radiation-induced cardiovascular disease

Mast cell deficient C57BL/6 KitW$^{SH/SH}$ mice and their wild type littermates (both fed a normal low-cholesterol diet) were whole-body irradiated at the age of 8 weeks with X-ray doses of 0, 0.05, 0.1 and 2 Gy. Groups of 10 mice per dose and time point were exposed. Animals were sacrificed at the age of 20 and 60 weeks and were examined for degenerative changes in the coronary arteries and aorta. Exposure of KitW$^{SH/SH}$ mice to any dose had no significant effect on lesion frequency or on average lesion size, regardless of the time of examination. Double mutant ApoE$^{-/-}$/ KitW$^{SH/SH}$ mice were irradiated with 0.1 and 2 Gy and examined 20-weeks and 6ß weeks post-irradiation. We conclude that mast cells are not required for the development of atherosclerotic lesions, but cannot exclude a role in other cardiovascular diseases. The proteome of heart tissue from mast-cell deficient (ApoE competent) mice were examined 20 weeks after irradiation by 0.05 Gy, 0.1 and 2 Gy. This showed that among quantified proteins 25, 21 and 60 proteins were significantly differentially expressed in irradiated hearts, respectively, compared to controls

($p<0.05$). Although the significantly deregulated proteins were not identical between the groups, they shared biological functions. The majority of the deregulated proteins were involved in the structural organization, acute phase response and mitochondrial function. The Ingenuity Pathway Analysis (IPA) showed that the network "Cardiovascular System Development and Function" was the most affected one in the irradiated heart after 0.05Gy and 2.0 Gy. IPA indicated radiation-induced metabolic disordering after 0.1Gy and 2.0 Gy. The alteration in cardiac cytoskeleton proteins was most pronounced after 2.0 Gy. IPA Toxicity and Disease analysis indicated the associations of the differently expressed proteins at higher doses with several cardiotoxicity groups such as cardiomyopathy (0.05Gy and 2.0 Gy), vascular disease (0.1 Gy) and hypertrophy (2.0 Gy). Proteomics analysis of the heart tissue 60 weeks after irradiation by 0.05 Gy, 0.1 and 2.0 Gy showed that among quantified proteins 18, 17 and 24 proteins were significantly differentially expressed in irradiated hearts, respectively, compared to controls ($p<0.05$). There were no shared proteins between all three profiles. However, the proteome profile of the 0.1 Gy-exposed heart shared 2 proteins with the 0.05 Gy profile (Collagen VI alpha and Cytochrome b-c1 complex subunit 7) and 3 proteins with the 2.0 Gy profile (Cytochrome c, Proteasome subunit alpha type-2 and Peptidyl-tRNA hydrolase 2). IPA analysis showed that mitochondrial dysfunction was the pathway mainly affected after irradiation. The network "cell to cell signalling" was the most affected one in irradiated heart after 0.05 Gy. "Cell survival" and "metabolism disordering" were affected after 0.1 Gy and 2.0 Gy, respectively. IPA Toxicity and Disease analysis indicated the associations of the deregulated proteins with heart inflammation after all three doses.

Quantitation of plaque area in the aorta of the double knockout mice as shown in Figure 11A revealed that the absence of mast cells had no impact on spontaneous development of atherosclerotic plaques in ApoE-/- mice. When ApoE-/- mice were irradiated, exposure to 0.1 Gy led to the increase in the area of the aorta that is covered by plaques, and this radiation-induced increase was also apparent in $ApoE^{-/-}$/ $KitW^{SH/SH}$ mice, which were devoid of mast cells, demonstrating that radiation-induced increase in plaque-covered area was not compromised by the lack of mast cells (Figure 11B). This conclusion is complicated by the observation of the 2Gy-irradiation mice as seen in Figure 11C, where irradiated ApoE-/- mice exhibited increase plaque-covered area of the aorta, but 2Gy-irradiated $ApoE^{-/-}$/ $KitW^{SH/SH}$ mice did not exhibit similar magnitude of increase. Since 0.1Gy-rradiated mice and 2Gy-irradiated mice showed different effect of mast cell absence, it is not possible to conclude unequivocally on whether mast cells are necessary for irradiation-induced atherosclerotic plaque formation. It is noteworthy that un-irradiated $ApoE^{-/-}$/ $KitW^{SH/SH}$ mice are equally susceptible to spontaneous atherosclerotic plaque formation as ApoE-/- mice (Figure 11A), which indicates that mast cells are not at all necessary for spontaneous plaque formation. If the 2Gy-irradiated mice results are re-producible, it would suggest that radiation-induced plaque formation is elicited through a different mechanism that that of spontaneous plaque formation, an attractive notion that would be worth further investigation especially when the proteomic results demonstrated that the protein changes induced by these two radiation doses are entirely different. The analysis indicated that the proteome profiles of different dose- and time points were distinct and had hardly any common protein components or pathways. The mitochondrial function, particularly oxidative phosphorylation, was the only signalling pathway that was significantly affected after all exposures and time points (Figure 13). In the absence of wild type mouse control for comparison, it is difficult to interpret the present observation optimally. In order to elucidate the effect of mast cell deficiency on heart structure and function after radiation exposure, the study on the irradiated wild type animals should be done.

3.4.3 Effect of radiation on interactions between endothelial and non-endothelial cells (PHE)

Having established the morphological and functional integrity of the 3D co-culture system as described in the previous report, and established a sensitive LDL ELISA assay, 3D co-cultures were prepared and X-irradiated at 0, 0.05, 0.1 and 2 Gy. After 1, 5, 7 and 14 days, LDL was added to these cultures followed by 4 hours of incubation in the incubator to allow for uptake of LDL. LDL remaining in the media was collected and their concentration measured using the LDL ELISA we established. The results show that radiation doses of 0.1 Gy and 2Gy exerted a modest and transient rise in the uptake of LDL from day 5 to 7. No difference in LDL uptake was detected in 0.05Gy-irradiated cells at all time points tested in multiple experimental repeats.

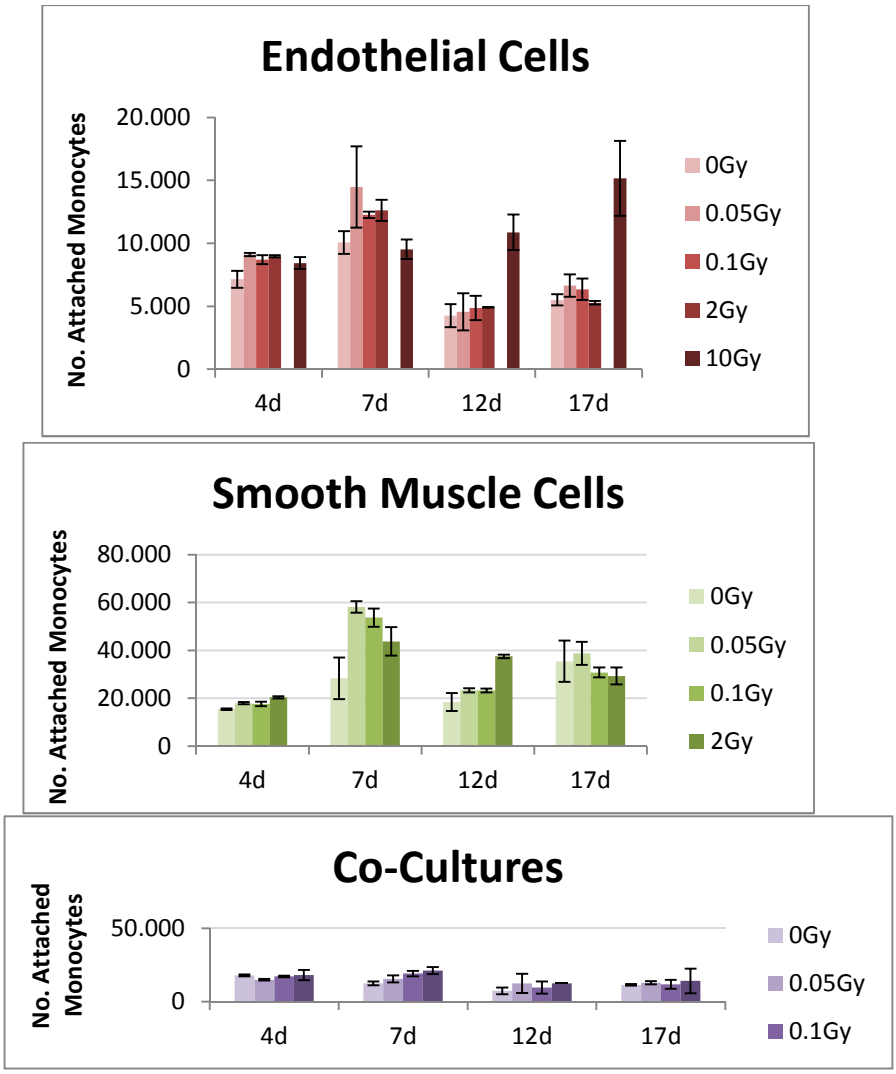

Figure 12: Effects of radiation on adhesion of monocytes on EC (top), SMC (middle) and 3D co-culture (bottom)

3.4.4 Monocyte attachment to endothelial cells in response to radiation

Infiltration of monocytes into the arterial wall is a multi-step process that begins with the attachment of monocytes to the endothelial cells. We devised a monocyte adhesion assay to test whether radiation would induce any changes to the adhesiveness of the endothelial cells for monocytes (Figure 12). Having established the robust linearity of the assay, we tested the effects of radiation on EC, SMC and 3D co-culture of EC+SMC. Figure 12 shows that for up to a week post-irradiation irradiation (up to 2Gy), EC exhibited a modest increase in adhesiveness. This is lost by day 12 and later. As a comparison, irradiation of EC with 10Gy X-ray induces a modest increase in adhesiveness that persists and even increases steadily up to 17 days (the latest time-point). A similar increase in adhesiveness is seen with SMC, with the exception that this effect is longer lasting but as seen with EC, this effect is eventually lost in time. It is notable that SMCs are significantly more adhesive than EC whether or not they were irradiated. When EC and SMC were cultured together in a 3D co-culture system, there was no measurable increase in adhesiveness up to 4 days post-irradiation but a dose-dependent increase was observed at 7 days post-irradiation. This increase is eventually lost by day 12.

The experiments above demonstrate that radiation can impose a transient effect on LDL uptake and monocyte attachment. These two properties are essential for the formation of atherosclerotic plaques. Although these effects are compelling and interesting, they are nevertheless not irrevocable evidence that radiation induces atherosclerotic plaques. This is because the formation of plaques is a time-consuming process that takes years. As the effects observed are only transient (lasting a few days), it is necessary to be conservative in our assessment of their relevance.

3.5 Search for biomarkers of radiation exposure

Both triage of radiation victims and molecular epidemiology studies require biomarkers capable of predicting outcome following radiation exposures. A number of DNA damage-based biomarkers already exist to quantify exposures relevant for cancer risk, but little is known about potential biomarkers of cardiovascular events relevant to radiation exposures. Our proteomic analysis of heart tissues derived from several of the experimental models is described elsewhere in this report.

Previous studies have demonstrated that a single local heart dose of 2 Gy results in persistent impairment of the mitochondrial respiratory function, increased oxidative stress and progressing structural alteration of the mitochondria-associated cytoskeleton both in both C57BL/6 and ApoE deficient mice. We have analysed the mitochondrial proteome responses of ApoE deficient mice after 15 and 300 days of **chronic** irradiation using a label-free mass spectrometry approach. Mitochondrial samples were digested with trypsin and analysed by mass spectrometry. Five biological replicates were used to quantify the protein alterations. The deregulated proteins were imported in Ingenuity Pathway analysis software (IPA) for analysis of significantly deregulated pathways and networks.

We quantified 935 and 842 proteins in the mitochondrial fraction after 15 and 300 days after exposure to cumulative doses of 0.3 Gy and 6 Gy, respectively. Two hundred fifty proteins were deregulated after 15 days of treatment (+1.3 fold, $p<0.05$). Three hundred days after the treatment we found 165 significantly deregulated proteins (1.3 fold, $p<0.05$). Thirty-three proteins were shared between the different treatments . Fifteen days after the treatment the most significantly deregulated protein pathways included mitochondrial dysfunction, fatty acid oxidation, amino acid metabolism (valine and isoleucine), TCA cycle and unfolded protein response. In all deregulated pathways, except for unfolded protein response, the proteins were significantly up-regulated suggesting that cardiac mitochondria responded to chronic irradiation by up regulation of the metabolic pathways. We have shown previously that immediately after acute total body irradiation many metabolic pathways showed upregulation in the heart tissue as a result of adapting to stress conditions.

Three hundred days after the treatment we identified mitochondrial dysfunction, oxidative phosphorylation and actin cytoskeleton signalling to be the most significantly deregulated pathways. In this case, all proteins from mitochondrial oxidative phosphorylation pathway were down-regulated. This analysis was in agreement with our previous study of acute irradiation on heart mitochondria in C57BL/6 and ApoE deficient mouse strain where persistent down-regulation of mitochondrial function and cytoskeletal components was observed. The proteins of mitochondrial respiratory chain were significantly up-regulated 15 days after the exposure, whilst at 300 days the mitochondrial respiratory chain proteins were down-regulated. We found some subunits of Complex I, III, IV and V to be down-regulated 300 days after the treatment (Figure 13). In our previous studies using local heart radiation (2 Gy) we found down-regulation of Complex I and III activity and amount, resulting in increased oxidative stress and decreased respiration. We therefore assume that similar effects are to be expected after 300 days of exposure to chronic low dose irradiation.

Acetylation of the lysine residue is a reversible posttranslational modification (PTM) that plays an essential role in the regulation of protein stability and activation of several signalling pathways. We have investigated whether the acetylation/de-acetylation process plays a role in the activation of known or novel pathways following a single acute radiation dose (2 Gy, 0.5 Gy and 0.2 Gy). For this purpose, we used primary human cardiac microvascular endothelial cells (HCMEC) and human coronary artery endothelial cell line (HCAEC) as cellular models.

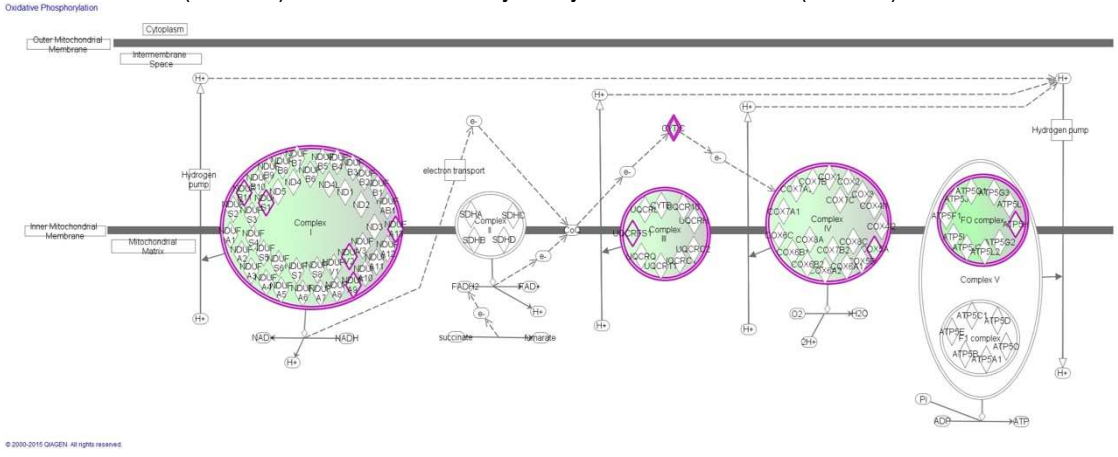

Figure 13 Proteome profile of the mitochondrial respiratory chain showing general down-regulation of Complexes I, III, IV and V after chronic irradiation (6.0 Gy, 300 days).

Radiation-induced effects on the HCMEC acetylome were investigated using a label-free proteomic quantification approach after enrichment of acetylated peptides. We identified 119 peptides, corresponding to 88 acetylated proteins, of which 54 were significantly changed in their acetylation status (fold change >1.30- or < 0.77). Four hours after irradiation 23 proteins were de-acetylated whilst 31 showed significant increase in the acetylation status. Proteins with a changed acetylation status were imported to GeneMANIA and IPA software tools for network analysis.

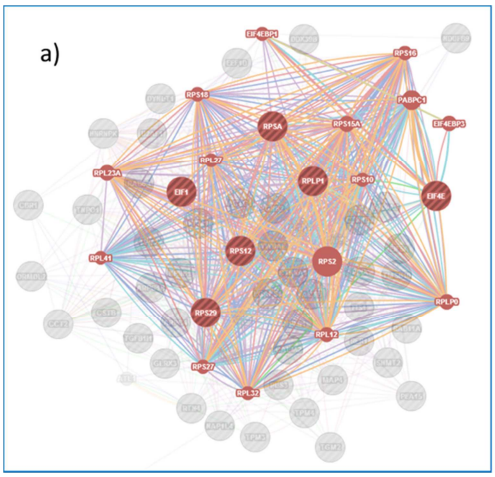

Figure 14 Pathway analysis of radiation-induced acetylated and de-acetylated proteins (2.0 Gy).

The imported proteins formed a large protein network according to the known interactions between these proteins in GeneMANIA database. The most significant clusters based on biological functions according to the number of affected proteins were identified. The analysis by GeneMANIA showed the initiation of translation to be the most affected pathway involving several proteins (6 deregulated proteins from the proteomics results and 15 predicted proteins) with a changed acetylation status as an early response to irradiation. The proteins involved in this network were ribosomal proteins and elongation initiation factors (Figure 14). The actin cytoskeleton signalling (5 deregulated and 4 predicted proteins) and nuclear transport (8 deregulated proteins and 1 predicted protein) were also indicated as affected by the GeneMANIA analysis. The most important biological processes identified by the IPA were cell death and survival, cellular movement, cellular development, cellular morphology and protein trafficking. The most significantly affected network was the stress-related response with extracellular-signal-regulated kinases (ERK; ERK1/2), p38 mitogen-activated protein kinases (p38 MAPK) and protein kinase B (Akt) as central hubs.

As many ribosomal proteins and elongation factors that were found to be de-acetylated in this study are putative sirtuin1 (SIRT1) targets we assessed its expression by immunoblotting. The level of SIRT1 was significantly up-regulated several-fold 4 hours but not 24 hours after irradiation (Figure 15).

Some mitochondrial proteins (cyclophilin A, fission 1 and NADH dehydrogenase (ubiquinone) 1 beta subcomplex, 9) were changed in their acetylation status after radiation exposure. Therefore, the level of the mitochondrial de-acetylated sirtuin 3 (SIRT3) was also studied 4 and 24 hours after irradiation. Figure 15 shows that, similar to SIRT1, SIRT3 was significantly up-regulated 4 but not 24 hours after radiation exposure.

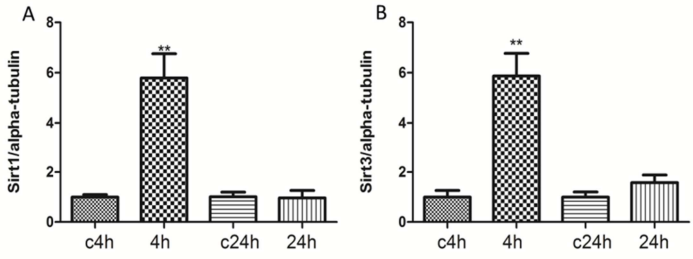

Figure 15 Immunoblot analysis of the SIRT1 and SIRT3 expression in primary HCMEC (2.0 Gy).

Radiation-induced effects on the HCAEC acetylome were investigated using label-free proteomic quantification after immune enrichment of acetylated peptides as described previously for HCMEC. Four hours after irradiation (0.5 Gy), 52 significantly deregulated acetylated proteins were identified ($p<0.05$, fold change >1.30- or < 0.77) of which 11 had increased and 41 decreased acetylation status. Twenty-four hours after irradiation, 91 proteins were significantly deregulated by acetylation ($p<0.05$, fold change >1.30- or < 0.77) of which 13 proteins had significant increase in acetylation and 78 decreased acetylation status. The overlap between the two time points was 44 proteins, with 5 proteins unique for 4-hour time point and 32 proteins for 24-hour time point. The direction of acetylation chance was the same in the shared proteins at both time points. Proteins with a changed acetylation status were imported to IPA for canonical pathway analysis. The analysis indicated that protein synthesis-related pathways (8 proteins), glycolysis (3 proteins) and integrin signalling (4 proteins) were the most affected pathways. Twenty-four hours after irradiation, protein synthesis stayed the most significantly altered pathway (12 proteins), followed by actin cytoskeleton, RhoGTPase and RhoA signalling pathways (8 proteins). Interestingly, 32 unique proteins found only at the 24-hour time point represented additional members of actin cytoskeleton, RhoGTPase and RhoA signalling but also calcium signalling.

3.6 Mathematical modelling

Estimation of the risks at low doses can be made using epidemiological data obtained from the study of effects at high doses, but this requires a mathematical extrapolation of the data. Current mathematical models for the fitting of epidemiological data use the two-hit clonal expansion model assuming linear no-threshold dose response. The parameters used are based upon concepts of gene mutation and carcinogenesis that clearly do not fit the biology of cardiovascular disease. We have pursued two complementary strategies to create more realistic mathematical models of cardiovascular disease. The first incorporates predicted biological processes identified as part of ProCardio.

RIVM has developed a mathematical model for the early stages of development of atherosclerosis in mice that can be used to test hypotheses on the role radiation plays in vascular plaque formation. To ensure that the model is radiobiologically sound, assumptions on the mechanisms that are essential to this complex process were formulated in collaboration with partners in ProCardio. Central to the model is the assumption that the effect of irradiation is an inflammatory response that leads to influx of macrophages and low density lipoproteins into the vessel wall, thus starting the process of plaque formation.

Plaque initiation is described as a stochastic process where exposure to ionizing radiation leads to a temporary increase in the initiation rate. The subsequent plaque growth is determined by the uptake of low density lipoproteins by macrophages in the vessel wall. We have formulated a system of ordinary differential equations describing the concentration of low density lipoproteins, the total capacity of macrophages to take up these low density lipoproteins and the resulting development of plaque size with time. We have written and validated a Fortran program that allows us to fit the model to experimental data, to test hypotheses on the role of radiation in plaque in atherosclerosis.

We have fitted this model to data of the Netherlands Cancer Institute (NKI, Fiona Stewart) (Figure 16). In experiments conducted at NKI, mice underwent acute exposure of the head and neck area (see Hoving et al. 2008 for more details). The plaque development model contains several parameters. For some parameter values, a reasonable estimate can be made based on information available in the literature. Values for the remaining parameters were determined by fitting the model to the measured plaque areas using a maximum likelihood approach. This did not lead to a unique optimal solution. Instead, we found several scenarios that are equally likely. An important conclusion that can be drawn from the model matched to the NKI data is that the model indicates that radiation has a dose dependent effect on the initiation of plaques. In the model for the NKI data, radiation does not influence the subsequent growth of plaques. Here, it should be noted that the experiments at NKI involved acute exposures only. Experimental data indicate (Tribble, 1999) that an inflammatory response to radiation persists for 1 or 2 weeks after exposure – a time window that is relatively short in comparison to the 40 week life span of the mice in the experiment. It is unlikely that a moderate change in the rate of plaque growth in the two weeks following an acute exposure would have a significant effect on the final volume of plaques. This could, however, be different for the mice that were chronically exposed in experiments in the ProCardio project. Matching the model (in a form that includes later stages of plaque formation) to these data could in the future elucidate dose-related effects on plaque growth.

Since in the model for mice acutely exposed at NKI radiation does not influence plaque growth, the size of a plaque follows a uniform growth curve. We have used this characteristic to test the performance of the model..

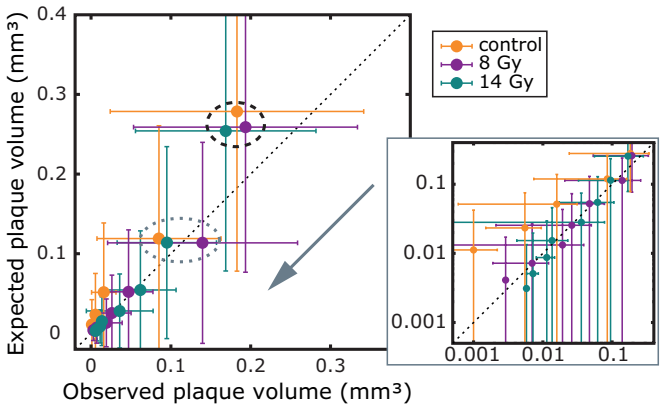

Figure 16: Observed and expected, modelled, volumes for ordered plaques. In the model for the NKI data, the size of a plaque size depends on the time since initiation only. We can, therefore, order plaques by age, or, equivalently, volume. Here, the youngest, and smallest, plaques are those closest to the origin: the arrow points in the direction of decreasing time since plaque initiation. The error bars show the standard deviation of the set of sorted plaque volumes, and indicate the range of corresponding volumes. For all three dose groups for which data were available, the model is in good agreement with the observations.

At the start of ProCardio it was planned to analyse the A-bomb survivor data (Shimizu 2010) with limited follow-up (1968-2003) for proximal survivors only. Because of an absence of any healthy survivor effect for the cerebrovascular diseases (CbVD) and heart diseases (Schöllnberger et al. 2015), it became clear that the full data set with follow up for the period 1968-2003, including distal survivors, would need to be analysed. In addition, two additional datasets (one for CbVD and one for heart diseases) were obtained from the colleagues at RERF that contain smaller doses categories at higher doses. The final set of non-nested models, which was found for the full dataset of Shimizu et al. (2010) and was used for multi-model inference (MMI), were then fitted to these two additional datasets to test whether possible nonlinear contributions to the dose-response relationship from MMI depend on the bin-size of the dose-categories. A prerequisite for MMI is the streamlining of the baseline function, which depends on sex, city, age attained and birth year. Starting from Preston's baseline model (Preston et al. 2003), the streamlining was performed in 2013/2014. Then, a larger set of different dose-response models was combined with the streamlined baseline model in the two possible mathematical ways, either as excess relative risk model (ERR-model) or as excess absolute risk model (EAR-model). These models were then fitted to the CbVD mortality data. The dose-effect modifiers age attained, age at exposure and sex were also tested for their statistical significance. An analogous procedure was performed using the heart diseases mortality data. For CbVD, the streamlined baseline model contains e.g. identical parameters for males and females and identical age at exposure-knots for males and females related to a parameter that marks the dependence on a quadratic spline function. Altogether, the baseline model contains 15 parameters. Table 6 shows the deviance difference, the number of model parameters and the Akaike weights (AIC-weights) for the preferable non-nested models. The ERR-LNT model contributes to the MMI with a weight of 0.29. No significant dose-effect modifiers were found. None of the EAR-models were statistically significant. years and an age at exposure of 30 years. Clearly, the dose-response from MMI predicts a stronger radiation effect at higher doses compared to the LNT model and a smaller radiation effect at lower doses; the LNT model over predicts the radiation risk below 1.3 Gy. At 0.1 Gy, for example, the LNT model over-predicts the risk by a factor of about 3. The reason for this is the contribution of the quadratic model to the MMI. No evidence for a threshold dose, D_{th}, was found consistent with Shimizu et al. (2010).

Table 6: The two preferable non-nested models for the LSS data on mortality from CbVD are provided. Here, Δdev denotes the deviance difference compared to the model with the smallest deviance (i.e. the one with the best fit). The number of model parameters is presented together with the AIC-weights. Both models contain 15 baseline parameters plus one parameter associated with the dose-response.

▪ Preferable dose-response models	▪ Δdev	▪ Number of parameters	▪ AIC-weight

▪ ERR-LNT model	▪ 1.76	▪ 15+1	▪ 0.29
▪ ERR-Q model	▪ 0	▪ 15+1	▪ 0.71

For mortality from heart diseases, the streamlined baseline model contains 20 parameters. ERR-models and EAR-models have comparable deviances (i.e. the values for ∆dev are small; Table 6). Evidence for a threshold dose was found from the ERR-step and EAR-step models and the EAR-linear-threshold model (EAR-LTH). Table 7 shows the seven preferable non-nested models together with their AIC-weights. Significant dose-effect modifiers were found for the EAR-LNT and EAR-Q models. For the step models a constant slope of 10/Gy was used. Figure 17 shows the dose-response relationship of the excess relative risk for mortality from heart diseases for an age attained of 70 years and an age at exposure of 30 years. The dose-response from MMI is dominated by the LNT model (AIC-weights of 0.31 and 0.22). The LNT model over-predicts the risk up to higher doses. This is because of the contribution of the quadratic model to the MMI. Due to the more comprehensive characterisation of model uncertainties the dose-response curve from MMI predicts that the risk for mortality from heart diseases is significant only at doses above 2.57 Gy (i.e. the 95% confidence intervals for MMI include zero risk up to 2.57 Gy). These results are consistent with those of an earlier analysis (Schöllnberger et al. 2012) that analysed the data from LSS Report 13 (Preston et al. 2003), restricted to proximal survivors and follow-up from 1968 to 1997.

The ProCardio-funded analyses showed that the threshold doses associated with the ERR-step and EAR-step models and the EAR-LTH model do not depend on the dose stratification of the grouped LSS data, i.e. on the cut-points of the dose categories. This result was obtained by fitting the two step models and the ERR-LTH model to a modified dataset for mortality from heart diseases, which was provided to ISS by colleagues at RERF. This dataset contains a smaller bin size in the dose range between 1.5 and 2.5 Gy compared to the original dataset (Shimizu et al. 2010). For example, for the ERR-step model the step occurs at D_{th} = 1.51 Gy when fitted to the altered dataset, compared to D_{th} = 1.52 Gy for the original dataset (Table 7). When fitting the EAR-LTH model to the original dataset D_{th} = 2.36 Gy was obtained (Table 7) compared to D_{th} = 2.41 Gy for the altered dataset.

Table 7: The seven preferable non-nested models for the LSS data on mortality from heart diseases are provided. Here, ∆dev denotes the deviance difference compared to the model with the smallest deviance (i.e. the one with the best fit). Threshold doses are denoted by D_{th}. All models contain 20 baseline parameters plus 1 to 3 parameters associated with the dose-response.

▪ **Preferable dose-response models**	▪ **∆dev**	▪ **Number of parameters**	▪ **AIC-weight**
▪ ERR-LNT model	▪ 1.29	▪ 20+1	▪ 0.31
▪ ERR-Q model	▪ 3.32	▪ 20+1	▪ 0.11
▪ ERR-step model, D_{th} = 1.52 Gy	▪ 2.44	▪ 20+3	▪ 0.02
▪ EAR-LNT model	▪ 0	▪ 20+2 incl. one significant dose-effect modifier	▪ 0.22
▪ EAR-Q model	▪ 0.55	▪ 20+2 incl. one significant dose-effect modifier	▪ 0.16
▪ EAR-LTH model, D_{th} = 2.36 Gy	▪ 1.07	▪ 20+2	▪ 0.13
▪ EAR-step model, D_{th} = 2.54 Gy	▪ 1.09	▪ 20+3	▪ 0.05

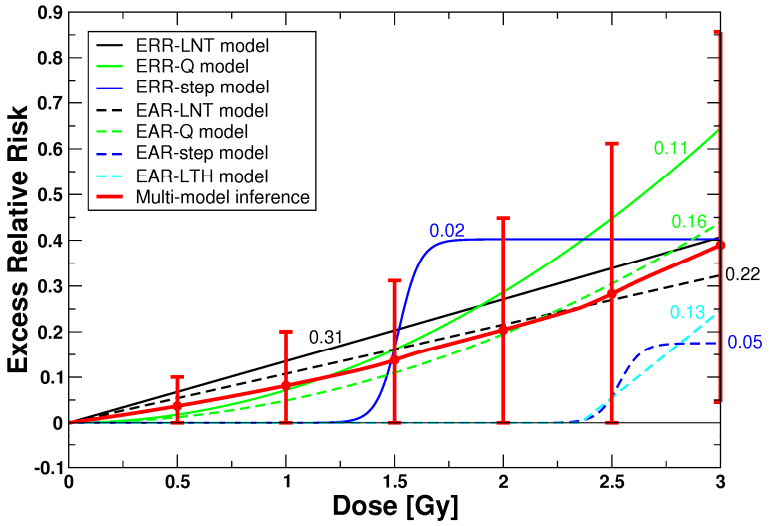

Figure 17: Excess relative risk versus absorbed dose for mortality from heart diseases for an age attained of 70 years and an age at exposure of 30 years. The AIC-weights for the seven non-nested models are shown. Error bars represent the 95% confidence intervals.

References

Alziar I, et al. Individual radiation therapy patient whole-body phantoms for peripheral dose evaluations: method and specific software. Phys Med Biol. 2009; 54: 375-83.

Diallo I,. et al. Estimation of the radiation dose delivered at any point in the body for individual patient in external beam radiotherapy. Radiotherapy and Oncology, 1996; 38:269-271.

Gallo, RL., et al. Endothelial cell surface alkaline phosphatase activity is induced by IL-6 released during wound repair. Journal of investigative dermatology 1997, (109) 4, 597-603.

Little MP et al. Review and meta-analysis of epidemiological associations between low/moderate doses of ionizing radiation and circulatory disease risks, and their possible mechanisms. Radiat Environ Biophys. 2010 May;49(2):139-53.

Preston DL,et al. Studies of mortality of atomic bomb survivors. Report 13: solid cancer and noncancer disease mortality: 1950–1997. Radiation Research 160:381–407, 2003

Schöllnberger H. et al. Dose-responses from multi-model inference for the non-cancer disease mortality of atomic bomb survivors. Radiation and Environmental Biophysics 51: 165-178, 2012

Schultz-Hector, S., & Trott RT. Radiation-induced cardiovascular diseases: is the epidemiologic evidence compatible with the radiobiologic data? International Journal of Radiation Oncology, Biology, Physics 2007, 67 (1), 10-18.

Shimizu Y. et al. Radiation exposure and circulatory disease risk: Hiroshima and Nagasaki atomic bomb survivor data, 1950–2003. Brittish Medical Journal 340:b5349, 2010

Testa, M. et al. Circulating levels of cytokines and their endogenous modulators in patients with mild to severe congestive heart failure due to coronary artery disease or hypertension. Journal of the American College of Cardiology 1996, (28) 4, 964-971.

Winther JF, et al . Childhood cancer survivor cohorts in Europe. Acta Oncol. 2015 May;54(5):655-68.

Wobus, A.M. & Löser, P., Present state and future perspectives of using pluripotent stem cells in toxicology research. Arch Toxicol.; 2011, 85(2) 79-117.

1.4 The potential impact

Socio-economic impact and the wider societal implications of the project

The risks of developing cardiovascular disease following a radiation exposure are well described for high doses (e.g. radiation therapy). For lower doses evidence for a deleterious effect exist, based on studies on atomic bomb survivors and nuclear workers, but here below 500mGy the evidence for a dose response relationship is weak. The risk of health effects in the dose range between natural background and 500mGy is that where society has the greatest need for definitive information on the risk to the cardiovascular system. The same problem also arises in considering effects of radiation on the brain, and hence PROCARDIO has been strategically and scientifically aligned with the EU project CEREBRAD, sharing information technology and concepts to create a synergy between the projects.

Our immediate goal was to determine possible mechanisms for the health effects of radiation by challenging conventional concepts of radiation-induced health effects. This approach assumes that conventional effects (misrepaired DNA damage, resultant gene mutation conferring a growth advantage, followed by clonal expansion of cells bearing a mutation) do not apply to cardiovascular effects. Consequently we have investigated alternative processes leading to new concepts, new mathematical descriptions of mechanistic processes and a fresh interpretation of the dose response relationship.

Contribution to Community and social objectives

The results of PROCARDIO are available as a publishable summary, as publications in the open scientific literature, as lecture material and as conference presentations. The results show important new evidence for the risks of cardiovascular diseases at low doses. These observations have implications for public health policy as mandated by radiation protection regulations across the European Community. We have made considerable effort to disseminate these findings to stakeholders, opinion formers, and through the work of several of the ProCardio scientists in national regulatory and advisory bodies.

Main dissemination activities and exploitation of results

The main dissemination route for scientific research remains publications in the open scientific literature. The successful publication of almost every aspect of ProCardio research is described in the publication lists below.

PROCARDIO activities have been disseminated to a number of policy-making bodies through our media activities, our presentations at scientific conferences (IRPA, RadRes, ERR, ICRR) and participation in EU policy making meetings (DoReMi, MELODI).

Outlook and future research

The results of ProCardio will be incorporated into the next edition of the Strategic Research Agenda for radiation protection research (MELODI workshop 2015). We will make a number of recommendations for future research, including:

1) Strengthening the epidemiological study of cancer survivors and expanding to include additional exposed cohorts (Tinea capitis children for example).

2) Working with PanCareSurFup to complete the large scale case-control study.

3) Experimental studies to obtain validation, in particular the anaylsis of radiation quality should be performed in vivo.

4) A second phase of chronic low dose exposures in vivo using the IES facility. Here the problem of keeping acute and chronic exposed animals under the same environmental conditions must be addressed.

5) A systems level study of the mechanisms of cardiovasculardamage after radiation, using the ProCardio information as a starting point (role of microRNA, long non-coding RNA, protein acetylation etc).

6) A study of the role of exosomal cargo in mediating both abscopal and bystander effects in cardiac model systems.